Could the tail be sufficiently long to allow the "trapped" continuum radiation to escape freely out the tail in regions of low solar wind plasma density downstream of Jupiter?

Because of limitations of the Voyager instrumentation, the electron distribution functions responsible for the $(n + 1/2)\, f_{ce}$ and f_{UHR} waves have not yet been determined. A basic question, therefore, remains as to why these waves are so closely confined to the magnetic equator. Is the equatorial confinement indicative of a highly anisotropic angular distribution that occurs only at the magnetic equator, or is the equatorial confinement a propagation effect? Can equatorial upper hybrid emissions account for the narrowband kilometric radiation by processes similar to the generation of the continuum radiation? Similarly, in the plasma sheet basic questions remain concerning the broadband electrostatic noise. How is this noise generated? Is the noise indicative of field-aligned currents linking the plasma sheet to the auroral ionosphere? If so, what role does this turbulence play in high latitude auroral processes? Does the noise produce sufficient anamolous resistivity to cause field-aligned potential drops, ion-acceleration, and plasma heating effects similar to the processes believed to be occurring in the terrestrial magnetosphere?

In conclusion, it is clear that the Voyager observations have added greatly to our knowledge of plasma wave and radio emission processes in the Jovian magnetosphere. Table 8.2 and Figure 8.22 summarize the many types of waves observed and their regions of occurrence. Although in most cases a first-order understanding is available to account for the generation of these waves, questions still remain concerning the possible role that these waves play in the physics of the Jovian magnetosphere.

ACKNOWLEDGMENTS

We would like to extend our thanks to W. Kurth, R. R. Anderson, and R. West for their assistance in preparing illustrations of the Voyager and ISEE data and for their helpful discussions concerning the interpretation of the data.

The research at The University of Iowa was supported by NASA through Contract 954013 with the Jet Propulsion Laboratory and through Grants NGL-16-001-002 and NGL-16-001-043 with NASA Headquarters and by the Office of Naval Research. The research at TRW was supported by NASA through Contract 954012 with the Jet Propulsion Laboratory.

9

THEORIES OF RADIO EMISSIONS AND PLASMA WAVES

Melvyn L. Goldstein and C. K. Goertz

A generally accepted theory of the enigmatic phenomenon of planetary radio emission is not yet available. In this chapter, we direct our attention primarily to the question of how the Jovian decameter radiation might be generated via both direct and indirect mechanisms. Direct mechanisms transform the free energy contained in an electron distribution (typically a loss-cone) directly into electromagnetic waves. Indirect mechanisms transform the free energy contained in an electron beam distribution first into electrostatic waves that can then couple, in some manner, to produce electromagnetic waves. The growth rates for the unstable electromagnetic and electrostatic waves are derived. Nonlinear theories are briefly discussed as they apply to the case of Jupiter's decametric radiation. Because most of the Jovian radio emission seems to be controlled by Io, we describe how Io, through the emission of kinetic Alfvén waves, can produce a "beamlike" electron distribution. It is more difficult to understand how Io can enhance or produce a "loss-cone" distribution. Thus we conclude that, at least for Jovian radio phenomena, indirect mechanisms are preferred. We also describe theories and models for the generation of the dynamic spectral arcs that characterize the radio spectrum from hectometric to decametric wavelengths.

9.1. Introduction

Jupiter is the most powerful planetary source of nonthermal electromagnetic radiation in the solar system, with a radio spectrum extending from a few kHz to over 100 MHz. The phenomenology of the decimeter component in the GHz range has been discussed in Chapter 7. Here we concentrate on the complex region of Jupiter's spectrum at decameter wavelengths, the so-called DAM. The relevant observations are described in Chapters 7 and 8 and we reference them freely.

Theoretical interpretations of Jupiter's low frequency radio emissions have been plentiful and imaginative, ranging from the suggestion by Vasil'ev, Volovik, and Zalyubovskii [1972] that extensive air showers of ultrarelativistic cosmic rays impinging on the Jovian atmosphere coherently excite the observed radio frequencies, to more prosaic proposals relating the observations to plasma instabilities well known from laboratory and space physics. However, owing perhaps to the rich and detailed phenomenology and fascinating morphology, or perhaps to our limited but rapidly increasing knowledge of the physical environment of Jupiter's magnetosphere and upper ionosphere, there are as yet no theories of any of the low frequency radio components that are generally accepted as being completely correct. This is in contrast to the situation at decimeter wavelengths, where, as pointed out in Chapter 7, a rather coherent picture of the emission mechanism has been formulated. As we shall see, however, some aspects of the observations at decameter wavelengths do appear consistent with at least some of the theories.

There is something of a renaissance of interest in this area of research as the results of the Voyager missions are digested and assimilated. In the following discussion, we emphasize the basic theoretical ideas that underly both the older and newer theories and models, and thus provide a suitable foundation for understanding the latest literature. In this chapter, we follow Smith [1976a] in using the term "phenomenology" to

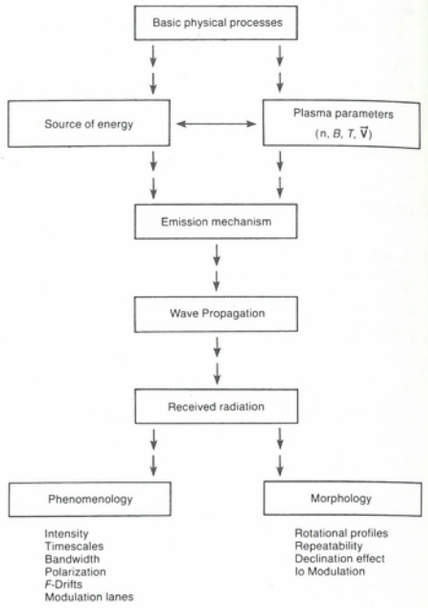

Fig. 9.1. A schematic view of the flow of information from the Jovian ionosphere, magnetosphere, and Io plasma torus to a remote observer. In many situations, the physical mechanisms for energy release in the plasma environment must be inferred from electromagnetic radiation that is detected far from the source region. Theoretical attempts to deduce the primary physical processes controlling the release of energy often proceed by trying to simulate nature by hypothesizing the existence of a source of free energy, then calculating the response of the system, and comparing the result to the observations.

refer to observables (intensity, polarization, frequency bandwidths, etc.), and in reserving "morphology" for interpretive organization of data such as, for example, occurrence probabilities. Generally, we will concentrate on theoretical work completed since Smith's review, referring to earlier work as necessary to make our discussion fairly self-contained.

In principle, the observed radiation may be used to study the relevant physical processes and diagnose the physical conditions (i.e., plasma parameters) at Jupiter. Figure 9.1 shows in a simplified manner the flow of information from Jupiter (its ionosphere, magnetosphere, or Io plasma torus) to a remote observer. By some physical process, a source of energy is released in a plasma. This energy causes radiation by the action of one or more emission mechanisms. If the radiation can propagate to the observer, information about the physical processes, energy exchange, and plasma environment can be obtained in a coded way. The decoding of this information is obtained by running back through the scheme of Figure 9.1. Evidently this inversion process can easily lead to serious errors because the number of unknown variables exceeds the number of observed independent parameters. Thus, theorists often go the other way, trying to simulate what happens in nature. Starting with a physical process, for example, the interaction of Io with the magnetosphere, they calculate the resulting free energy (residing either in spatial or velocity-space inhomogeneities of the plasma distribution). Once the sources of free energy have been identified, one tries to estimate the efficiency by which this energy is transformed into observable radiation. Sometimes, but not always, propagation and refraction of the radiation through the often inhomogeneous medium between the source and observer is calculated.

A few general comments about the decameter observations can be made before getting into detailed theoretical formulations. Some of these comments have been made before [Smith, 1976a], but are worth repeating. The high intensities, limited bandwidth, short timescales, and sporadic nature of the radio emissions indicate that they are due to stimulated emission from plasma microinstabilities. In addition, the remarkable repeatability of many of the decameter and kilometer wavelength spectra

imply a long term stability of at least some of the plasma parameters. However, much variability is still present, including source drifts in longitudes by up to 10°. Although the basic plasma parameters may be stable over long periods of time, it must be stressed that the decameter radiation is not always observed even when the viewing geometry is propitious. This is apparently because of variations in the intensities and frequency bandwidths of the various sources; the Planetary Radio Astronomy (PRA) experiment on Voyagers 1 and 2 demonstrated that at sufficiently low signal strengths the occurrence probability in CML is nearly unity at almost all longitudes at some frequency (cf., Fig. 7.11). This is true of both the Io phase-independent and phase-dependent components. The variations in intensity and bandwidth are, however, significant, indicating that there must be some variable and random influence on the propagation characteristics of the medium, emission mechanism, or physical processes that generate the free energy. The distinguishing characteristics of the Io phase dependent and independent sources are described in detail in Chapter 7 (in particular see the discussion of Fig. 7.8).

Nearly all of the decameter radiation appears to be controlled by Io in some manner. Apparently either Io itself, or its plasma torus, modifies the plasma distribution (in configuration or velocity space) in such a way that free energy is converted into electromagnetic waves. In addition, Io probably enhances or creates sources of free energy, thus accounting for the greater intensities of some of the Io-controlled sources in comparison with the Io-phase-independent sources. It has become increasingly clear from both ground-based and space probe studies of the plasma torus that Io is ultimately responsible for many, if not all, of the dynamical phenomena in the inner Jovian magnetosphere. Hence, the traditional division in decameter morphology between Io-independent and Io-controlled sources is something of a misnomer. Evidently the essential distinction is whether or not the particular decameter phenomenon is correlated with the phase of Io. Thus, we will occasionally refer to the DAM sources as being either Io-phase independent or Io-phase dependent.

The repeatability of DAM and HOM spectra suggests that the frequencies are related to a characteristic frequency of the plasma. The possibilities are the electron and ion cyclotron frequencies, plasma frequencies, and upper- and lower-hybrid frequencies. The characteristic ion frequencies and the lower-hybrid frequency, are too low to control the emission of megahertz electromagnetic waves, although in Section 9.3 we will see that these low frequency waves may play a crucial role in the chain of events leading to the observed electromagnetic radiation. The highest electron number densities inferred from radio occultation measurements [Fjeldbo et al., 1975, 1976; Eshleman et al., 1979a,b; Chap. 2] correspond to $f_{pe} \simeq 3$ MHz, which not only excludes Langmuir waves as the source of the decameter emissions, but also implies that the electron cyclotron frequency and upper-hybrid frequencies are very nearly equal. Thus, only the electron cyclotron frequency and upper-hybrid frequency appear to be directly related to the observed spectra.

The argument that the observed radiation is the upper-hybrid or electron cyclotron frequency at the source suggests that the maximum frequency of the Io controlled DAM (39.5 MHz) then corresponds to the maximum magnetic field at the foot of Io's flux tube (IFT), which is inferred from Pioneer 11 observations [Smith, Davis, and Jones, 1976; Acuña and Ness, 1976a; and Chap. 1] to be approximately 14 G in the northern hemisphere. Consequently, any electrons reaching these high fields must have pitch angles inside the steady state loss-cone. We are thus led to the immediate conclusion that stably trapped electrons cannot produce cyclotron frequency radiation at the highest decameter frequencies unless the exciters have been scattered into the

loss-cone and/or have been accelerated somewhere along the northern half of the Io flux tube. For this reason, generation mechanisms involving trapped electrons have been proposed only in connection with the Io-phase independent sources [Goldstein and Eviatar, 1979]. Analysis of Voyager PRA data indicates that the historical distinction between the frequency range of the Io-phase independent and Io-phase dependent sources that was based primarily on ground-based observations may actually be a manifestation of differences in the intensities of the two sources as first suggested by Desch [1976]. Barrow and Alexander [1980] and Barrow and Desch [1980] report that the upper-frequency limits of the Io-independent source B can reach 36–38 MHz, very close to the highest observed frequencies of the Io-dependent source (39.5 MHz). For a more complete description of the morphology and phenomenology of these and other aspects of DAM, we refer the reader to Chapter 7.

When the waves are observed, they appear at frequencies much higher than the electron cyclotron frequency at the observer, thus the waves are high frequency waves. In a magnetized plasma there are two high frequency normal modes [Stix, 1962]: the ordinary (O) and the extraordinary (X) mode. The X mode consists of two branches, a slow mode for which the phase velocity is less than the velocity of light (also called the z mode or band II); and a fast mode for which the phase velocity is larger than c (also referred to as band III or simply the X mode). Between the two branches there is a "stop band" where the electromagnetic X-mode wave becomes evanescent and cannot propagate. Consequently, the slow X mode cannot easily escape from Jupiter. For the ordinary mode there is no stop band above the local electron plasma frequency. Therefore, far from Jupiter the observed radiation must be in either the fast X mode or O mode. Observations indicate that the observed radiation is X mode. However, this does not prove that it is generated in that mode because strong mode coupling between the point of observation and the source is possible.

We can summarize the theoretical problem of decameter radio waves as follows: by what sporadic mechanisms is the plasma distribution modified so that its free energy is converted with adequate efficiency into electromagnetic waves near the local electron cyclotron frequency and how does this radiation propagate through the intervening plasma (including the Io plasma torus) to a distant observer? One of the keys to answering this question is the in situ form of the electron distribution function. This is not easily determined, primarily because there are no observations of the electron distribution in the suspected source region, the Jovian ionosphere. Much of our discussion below will concentrate on the question of what clues are contained in the extant observations that permit models of the distribution function to be constructed. Because the Io flux tube appears to be the likely location of the energetic electrons that generate the decameter radiation, we discuss several properties of that region that can give rise to unstable distributions. Several theories for the emission process yield similar observable characteristics, even though they require quite different distribution functions. We try to distinguish those aspects of the various theories that seem more plausible than others.

The various theories can be distinguished by whether they depend on direct or indirect emission processes. The term "direct emission" refers to particle-generated electromagnetic waves; whereas the term "indirect emission" refers to wave-wave interactions and scattering (mode conversion). Until recently most of the literature dealing with Jovian emissions has concentrated on direct linear emission mechanisms. In contrast, the terrestrial kilometric radiation (TKR), which is similar in many respects to Jovian radiation, has spawned several nonlinear theories of its generation. Similar theoretical tools are now being applied to Jupiter's radio sources.

In the following section, we review the linear plasma theory that has been utilized in constructing "direct emission" theories, and follow that with a review of several applications to the DAM problem. In Section 9.3 we review some of the techniques used in nonlinear (indirect) emission theories and emphasize applications to Jupiter. Much of the theoretical formalism we develop is also useful for discussions of a number of other Jovian radio and plasma phenomena besides DAM. In Chapter 12, the linear instability formalism is employed to describe several microscopic plasma processes that give rise to particle diffusion and whistler wave generation.

In several instances, newly discovered components of Jupiter's radio spectrum, in particular, the nKOM and bKOM components described in Chapter 7, are only just beginning to inspire theoretical attention, and thus a "review" would be premature. We have therefore chosen to concentrate on the microscopic conditions that can produce DAM. Furthermore, we emphasize work that has been completed since Smith's excellent review [Smith, 1976a], at the risk of being perhaps too uncritical of work that has been available to us only in preprint form. Where possible, we try to relate the formalism to such macroscopic phenomena as occurrence probability and source location, but we make no claims of completeness.

9.2. Linear theories

Direct emission mechanisms

Plasmas are characterized by a multitude of instabilities that occur if free energy, stored in thermal energy, kinetic energy, ordered motion, potential mechanical energy, electrostatic energy, etc, exceeds a critical level and becomes transformed into other forms including radiation. In a typical situation, a small perturbation in some plasma parameter, or a spontaneously emitted plasma wave, grows exponentially with time ($\sim \exp \gamma t$), that is, the temporal change of the perturbation is proportional to the perturbation itself. When the growth rate for waves is positive ($\gamma > 0$), we speak of coherent or stimulated emission. In this section and in the appendix, we derive general expressions for the linear growth rate of various wave phenomena, both electromagnetic and electrostatic that are then used here, in Section 9.3, and in Chapters 8 and 12. For an alternative point of view to the one we present, the interested reader should refer to Kennel and Wong [1967] and Baldwin, Bernstein, and Weenik [1969]. Both those references proceed from the linearized Vlasov equation and include all wave modes and directions of propagation. The derivation by Melrose [1968] and Harris [1968] is also general in that all wave modes and directions of propagation are included, but is couched in terms of the semiclassical theory of emission and absorption of waves. Thus, both stimulated and spontaneous emission can be included in a straightforward way. In the Vlasov treatment, the inclusion of spontaneous emission is not at all a trivial exercize, and the reader is referred to Wu [1968] for details. In the following discussion, we use the approach and notation of Melrose [1968].

We treat a homogeneous magnetized plasma which is both gyrotropic (i.e., the distribution functions are assumed to be independent of azimuthal direction about the magnetic field [see, for example, Montgomery and Tidman, 1964]) and collisionless. Wave amplitudes are assumed to be small enough to leave the particle orbits essentially unperturbed. The waves are harmonic and are not significantly damped by the background medium. We deal only with the normal modes that exist in a (cold) magnetized plasma containing no free energy. The normal modes of interest to us here and in Section 9.3 include the upper- and lower-hybrid electostatic modes, and the ordinary and extraordinary electromagnetic modes. The addition of a population of parti-

cles not in thermal equilibrium introduces a non-Hermitian part to the dielectric of the medium. It is this part that implies growth (or damping). In principle, observations (Chap. 7) could determine which mode the radiation is in, and theory could determine the form of the distribution function needed to amplify that mode. As we shall see, however, the situation is rarely that simple. Various theoretical mechanisms are capable of generating the same wave mode, and often, unless the source location is known with some precision, observations are incapable of determining the original wave mode at the source.

The linear growth rate γ for arbitrary direction of propagation and for all polarizations is derived in the appendix and is given by

$$\frac{\gamma^{\pm}(k)}{\omega} = \sum_{\nu} \frac{2\pi^2 q^2 c^2}{\omega^2 |k_{\parallel}|} k_{\parallel} n^{\pm} \int dp_{\parallel} \cdot \int dp_{\perp} p_{\perp}^{2} \delta(p_{\parallel} - p_{\parallel 0}) \frac{\theta_{\nu}^{\pm} G_{\nu}^{\pm} f^{\pm}(p_{\perp}, p_{\parallel})}{(m^2 c^4 + p^2 c^2)^{1/2}} \tag{9.1}$$

where

$$\theta_{\nu}^{\pm} = |J_{\nu\pm 1}(z) E_{\mathrm{R}} + J_{\nu\mp 1}(z) E_{\mathrm{L}} + (2)^{1/2} \frac{v_{\parallel} k_{\perp}}{v_{\perp} |k_{\perp}|} J_{\nu}(z) E_{\parallel}|^2 / W(k_{\perp}, k_{\parallel}) \tag{9.2}$$

indicates the polarization of the particular mode under consideration, and

$$W = (|E(\mathbf{k})|^2 \omega \, \partial\Lambda/\partial\omega) / (4\pi\lambda_{ss})$$

is the wave energy as a function of parallel ($k_{\parallel}$) and perpendicular wave number ($k_{\perp}$). E is the wave electric field strength. The subscripts R and L refer to right-handed and left-handed electromagnetic modes, and the subscript $\parallel$ refers to the longitudinal polarization of the electrostatic modes. Note that the magnitude of $E(\mathbf{k})$ cancels in (9.2), as it should. Λ, λ_{ss} as well as the other notation follows Melrose [1968] and is defined in the appendix.

The sign of the growth rate is determined by the operator G which acts on the particle distribution function. G is given by

$$G_{\nu}^{\pm} = \left[k_{\parallel} p_{\perp} \frac{\partial}{\partial p_{\parallel}} + (\omega\gamma_r m^{\pm} - k_{\parallel} p_{\parallel}) \frac{\partial}{\partial p_{\perp}} \right] \tag{9.3}$$

Amplification ($\gamma > 0$) is only possible if $G_{\nu}^{\pm} f(\mathbf{p}) > 0$ for some values of $\mathbf{p}$. The interpretation of this criterion is given below.

The resonance condition for the parallel momentum in (9.1) can be written as

$$p_{\parallel 0} = \gamma_r^{\pm} m^{\pm} \beta_{\parallel 0} c = [1 - \nu\omega_c^{\pm}/\gamma_r^{\pm}\omega] (\omega/k_{\parallel}) m^{\pm} \gamma_r^{\pm} \tag{9.4}$$

or

$$v_{\parallel 0} = (\omega/k_{\parallel}) (1 - \nu\omega_c^{\pm}/\gamma_r^{\pm}\omega)$$

where $\gamma_r = (1 - v^2/c^2)^{-1/2}$ is the Lorentz factor and the phase velocity of the wave along the magnetic field is $\omega/k_{\parallel}$. The $\pm$ superscript refers to contributions from ions (+) or electrons (−).

We can now specify general rules concerning properties of the distribution function necessary for amplification. The delta function in (9.1) indicates a resonance condition

that requires that the Doppler-shifted wave frequency must approximately equal ν times the relativistic cyclotron frequency of the resonant particle. The integer ν indicates the change of perpendicular energy of a particle upon emission of a photon. If $\nu = 0$, the change is zero, which is the well-known Cerenkov emission, or Landau resonance, in which only the parallel energy of the particle is changed. The resonances for $\nu \neq 0$ are known as cyclotron (or gyro-) resonances. Positive ν, corresponding to a decrease of $p_{\perp}$, is called the normal Doppler effect; whereas negative ν corresponding to an increase of $p_{\perp}$, is called the the anomalous Doppler effect. From the form of G we find that Cerenkov emission is amplified only if the distribution function has a positive slope in $p_{\parallel}$, that is, satisfies a Penrose criterion [Penrose, 1960]. We call these distributions beamlike because such distributions contain free energy in the parallel velocities and more particles can feed energy into waves than absorb energy from them. This situation is equivalent to population inversion in maser theory except that the population levels in the plasma are continuous.

For positive ν we can get amplification from either a beamlike distribution with excess free energy parallel to the magnetic field **B**, or a loss-cone type distribution with more free energy perpendicular to **B**. The loss-cone distributions contain more particles feeding energy into the wave (when $p_{\perp}$ decreases) than absorbing energy from the wave (when $p_{\perp}$ increases). Such distributions are equivalent to the population inversion of a maser. In both cases the population levels are quantized, although for all practical purposes in the loss-cone situation the quantization step $\Delta p_{\perp}^{2} = qB/c\hbar$ (see Eq. A.13) is negligible. The distribution can therefore be considered continuous in $p_{\perp}$. Similarly, for the anomalous Doppler-shifted emission, instability can result from either a beamlike or an antiloss-cone distribution.

If we use the resonance condition (9.4), G can be rewritten as

$$G_{\nu}^{\pm} f^{\pm}(p_{\perp}, p_{\parallel}) = \left[k_{\parallel} p_{\perp} \frac{\partial}{\partial p_{\parallel}} + \nu\omega_c^{\pm} m^{\pm} \frac{\partial}{\partial p_{\perp}} \right] f^{\pm}(p_{\perp}, p_{\parallel}) \Big|_{p_{\parallel} = p_{\parallel 0}} \tag{9.5}$$

The instability conditions for electrons can then be explicitly summarized as follows:

For the Landau resonance, $\nu = 0$:

$$\left. \frac{\partial f}{\partial p_{\parallel}} \right|_{p_{\parallel} = p_{\parallel 0}} > 0 \qquad \text{“beam”}$$

For the “normal” Doppler resonance, $\nu > 0$:

$$\left[p_{\perp} \frac{\partial}{\partial p_{\parallel}} + \frac{\nu\omega_{ce}}{\omega} m v_{ph} \frac{\partial}{\partial p_{\perp}} \right] f \Big|_{p_{\parallel} = p_{\parallel 0}} > 0 \qquad \begin{array}{l} \text{“loss-cone”} \\ \text{and/or} \\ \text{“beam”} \end{array}$$

For the “anomalous” Doppler resonance, $\nu < 0$:

$$\left[p_{\perp} \frac{\partial}{\partial p_{\parallel}} - \frac{|\nu|\omega_{ce}}{\omega} m v_{ph} \frac{\partial}{\partial p_{\perp}} \right] f \Big|_{p_{\parallel} = p_{\parallel 0}} > 0 \qquad \begin{array}{l} \text{“anti-loss-cone”} \\ \text{and/or} \\ \text{“beam”} \end{array}$$

Whether a distribution is a loss-cone or antiloss-cone is determined by the sign of $\partial f/\partial p_{\perp}$ at resonance, that is,

$$\left.\frac{\partial f}{\partial p_\perp}\right|_{p_\parallel = p_{\parallel 0}} \begin{array}{ll} > 0 & \text{loss-cone distribution} \\ < 0 & \text{antiloss-cone distribution} \end{array} \tag{9.6}$$

Obviously, an extensive study of (9.1) is beyond the scope of any single review. Instead of attempting to describe all possibilities, we restrict ourselves to two extreme cases: exactly parallel propagation ($k_\perp = 0$) and nearly perpendicular propagation ($k_\parallel \simeq 0$). The discussion of these two cases will serve to illustrate the basic principles of the linear analysis and introduce the sometimes confusing terminology used in the literature. For detailed investigations including obliquely propagating waves the reader is referred to appropriate references. An example of beamlike distributions unstable at both the Landau and normal Doppler resonances to the excitation of electrostatic waves ($E_\parallel$) is described in Section 9.3. Other examples dealing with electromagnetic waves are referred to below and are also treated in Chapter 12.

Parallel propagation

Let us look at the case of the parallel or quasiparallel propagating waves. In this case the argument of the Bessel functions in $\theta_\nu^{\pm}$ equals zero. Therefore, electrons can resonate with longitudinally polarized waves only when $\nu = 0$ (because only J_0 is nonzero if $z = 0$). Similarly, electrons resonate with right hand (RH) polarized waves if $\nu = 1$ and with left hand (LH) polarized waves if $\nu = -1$. In Section 9.3, we discuss an example where the $\nu = 0$ resonance excites obliquely propagating longitudinal waves. However, for exact parallel propagation, γ is zero because the term $\partial\Lambda/\partial\omega$ in W approaches infinity when evaluated at the solutions of the normal mode cold plasma dispersion relation.

From (9.1), (9.2), and (9.4) it would appear that the anomalous Doppler resonance ($\nu = -1$) can give rise to linearly unstable LH polarized ordinary mode waves. However, because $\nu < 0$, the resonance condition shows that the parallel resonance velocity is larger than the phase velocity. The phase velocity of the ordinary wave is itself almost always larger than c for frequencies of interest (i.e., $\omega \geq \omega_{ce}$) so that no resonance is possible. This is most easily seen from the cold plasma dispersion relation for the parallel propagating O mode, which is given by [Stix, 1962]

$$n^2 = k_\parallel{}^2 c^2/\omega^2 = \frac{(\omega - \omega_R)(\omega + \omega_L)}{(\omega - \omega_{ci})(\omega + \omega_{ce})} \tag{9.7}$$

where the left hand cut-off frequency is defined by

$$\omega_L = -(1/2)\omega_{ce}\{1 - [1 + 4(\omega_{ce}\omega_{ci} + \omega_{pe}{}^2)/\omega_{ce}{}^2]^{1/2}\}$$

and the right hand cut-off frequency is defined by

$$\omega_R = -(1/2)\omega_{ce}\{1 + [1 + 4(\omega_{ce}\omega_{ci} + \omega_{pe}{}^2)/\omega_{ce}{}^2]^{1/2}\}$$

The dispersion relation is illustrated in Figure 9.2.

In contrast, amplification of both the slow and fast branches of the X mode is possible via the normal Doppler resonance, $\nu = 1$. On the slow branch ($\omega < \omega_{ce}$), $p_{\parallel 0}$ and v_{ph} have opposite signs (see 9.4) and the amplified waves propagate backwards relative to the beam. As is true of all waves produced on the slow X-mode branch, this radiation cannot freely escape from the source because of the existence of an evanescent stop zone where the wave frequency becomes imaginary. The existence of this stop zone is apparent from this dispersion relation for the parallel propagating X mode [Stix, 1962]:

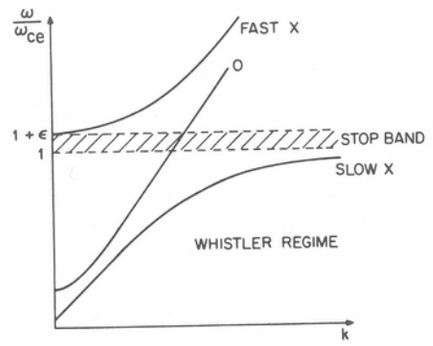

Fig. 9.2*a*. Dispersion relation for parallel propagating electromagnetic waves. The parameter $\epsilon = \omega_{pe}{}^2/\omega_{ce}{}^2$ is assumed to be small.

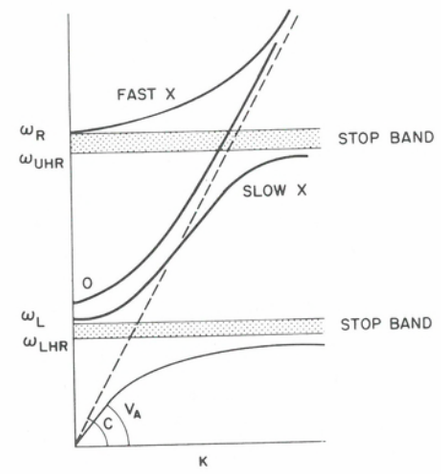

Fig. 9.2*b*. Dispersion relation for perpendicular propagating modes.

$$n^2 = \frac{k_\parallel{}^2 c^2}{\omega^2} = \frac{(\omega - \omega_R)^2}{(\omega + \omega_{ci})(\omega - \omega_{ce})} \tag{9.8}$$

This dispersion relation is also illustrated in Figure 9.2. The "whistler" mode lies on the slow branch ($\omega < \omega_{ce}$). Between ω_{ce} and ω_R, the evanescent band ($n^2 < 0$) inhibits the escape of the slow mode. Smith [1976b] has investigated the escape of the slow mode by tunneling through the stop zone and has shown that while this may be possible for radiation below 20 MHz,it is unlikely to occur at higher frequencies.

Another difficulty with backward propagating waves is that because the frequency is close to ω_{ce} they can resonate with thermal electrons and be damped. At the top of the Jovian ionosphere the ambient electron temperature has been estimated by Atreya, Donahue, and Waite [1979] to be 0.1 eV, and the effects of damping in the high frequency source region can be important in some situations (cf. Section 9.3). This mechanism can thus produce whistler mode waves at $\omega < \omega_{ce}$ [see, for example, Chang, 1963]. Observations of whistlers have been reported at Jupiter near $L = 8$ in the equatorial plane at the outer edge of the Io torus [Coroniti et al., 1980a] and are discussed in some detail in Chapters 8 and 12. Growth rates have been calculated using Equation (9.1) [Sentman and Goertz, 1978]. Because the direction of propagation is nearly parallel to **B**, one has no way of knowing if similar radiation is produced near the foot of the Io flux tube without actually placing a receiver in the high-latitude Jovian ionosphere.

From Equation (9.4), we see that on the fast branch ($\omega > \omega_R$) amplified waves propagate forward relative to the particles. Then, because both the density and magnetic field increase with decreasing distance from Jupiter, a wave initially produced above the local cut-off frequency by downward moving electrons will soon propagate into a region where $\omega \simeq \omega_R$, be reflected, and escape the Jovian magnetosphere. Of course, if a particle distribution is directed away from the planet, the wave can escape directly without reflection. However, because **k** is parallel to **B**, such escaping radiation would not in general reach an observer located near the ecliptic plane, and therefore, nearly parallel propagating waves are unlikely to be the source of the decameter radiation.

Perpendicular propagation

For perpendicular or quasiperpendicular propagation, the restrictions on ν are not as severe. This can be seen by setting $k_\parallel = 0$ in (9.1). For the normal Doppler effect ($\nu > 0$), a loss-cone distribution ($\partial f/\partial p_\perp > 0$) is required for amplification, independent of the mode considered. For the anomalous Doppler effect ($\nu < 0$), amplification requires an antiloss-cone distribution ($\partial f/\partial p_\perp < 0$), again independent of mode. However, anomalous Doppler effect interactions at exactly perpendicular propagation are unlikely because the resonance energy required is infinitely large. For the Landau resonance ($\nu = 0$), instability requires a beamlike distribution $\partial f/\partial p_\parallel > 0$).

For a variety of reasons, one of the most frequently hypothesized mechanisms for producing DAM is that of directly amplifying fast X-mode waves propagating nearly perpendicular to **B**. The advantages of such a scheme are obvious: the observed radiation is inferred to be X-mode, compilations of occurrence probability and identification of the two distinct sources (A and B; or Main and Early, respectively – see Chap. 7) certainly suggest (but do not require) that the emission pattern be a thin conical sheet with half angle ψ close to 80° [Dulk, 1965]. This would result naturally from waves excited nearly orthogonal to **B**. Furthermore, direct amplification of the fast X mode eliminates such complications as tunneling and mode conversion. Various versions of such mechanisms have been described by Twiss and Roberts [1958], Twiss [1958], Hirshfield and Bekefi [1963], Fung [1966a,b,c], Goldreich and Lynden-Bell [1969], Melrose [1976], Wu and Freund [1977], and Goldstein and Eviatar [1972, 1979] [Ben-Ari, private communication, has reported an error in the instability analysis in this last reference; consequently we will not discuss that aspect of those two papers]. These references consider instabilities driven by excess perpendicular particle energy arising from either loss-cone distributions, Dirac delta functions in $p_\perp$, or temperature anisotropies.

The cyclotron maser instabilities are examples of the loss-cone driven instabilities discussed above [see, for example, Wu and Lee, 1979; Lee, Kan, and Wu, 1980]. They have been invoked frequently as the excitation mechanism of DAM. However, many of the recent applications of this class of instabilities have been directed toward explaining TKR. In the TKR source it is often assumed that the ambient plasma density n_e is so low that the density of the energetic distribution n_b exceeds it by a large factor [Wu and Lee, 1979; Lee, Kan, and Wu, 1980]. In contrast, while the Jovian source region is also underdense ($\omega_{pe} << \omega_{ce}$), it has generally been assumed that n_e is still large ($\simeq 10^5$ electrons/cm^3), so that $n_e/n_b >> 1$. Lee and Wu [1980] have studied the instability for finite values of n_e/n_b. They computed the growth rate for both the slow and fast extraordinary modes as well as for the ordinary mode from Equation (A.24) or (9.1) using a loss-cone distribution function of the form $F(v_\perp, v_\parallel) = F(v_\perp)F(v_\parallel)$, where

$$F(v_\perp) = \frac{1}{\pi \beta_\perp{}^2} \left(\frac{v_\perp}{\beta_\perp}\right)^{2\alpha} \exp\left(-\frac{v_\perp{}^2}{\beta_\perp{}^2}\right)$$

$$F(v_\parallel) = \frac{1}{(2\pi)^{1/2} V_\parallel} \exp\left[-\left(\frac{v_\parallel - v_0}{2 v_\parallel{}^2}\right)^2\right]$$

and $\beta_\perp{}^2 = 2T_\perp/\{m_e(\alpha + 1)\}$. The growth rates for both the fast and slow extraordinary modes peak just above ω_R and just below ω_{ce}, respectively. In general, the growth of the slow mode, the one that cannot escape because of the stop zone, greatly exceeds that of the fast mode because the resonance velocity for the slow mode is less than that of the fast mode, which allows many more particles to participate in amplification of the slow mode. The question of whether substantial growth of fast mode waves can actually occur before the instability saturates because of the much faster growth of slow mode waves has not been addressed. The O mode is also unstable, but is not competitive with the two extraordinary mode waves.

The growth of the slow mode waves is related to the excitation of the Weibel instability [Weibel, 1959], which arises from an axial bunching of the energetic electrons (the cyclotron maser instability arises from an azimuthal bunching). Lee and Wu comment that at lower phase velocities the slow mode instabilitiy becomes a Weibel instability. This poses a potential difficulty with the cyclotron maser mechanism. Chu and Hirshfield [1978], in their comparative study of the two types of instabilities, concluded that they were both simultaneously present and always competed with one another. This means that only one branch can be unstable for a given value of $k_\parallel$. In general, the cyclotron maser instability tends to dominate for small $k_\parallel$, which would tend to produce conical emission patterns. Even ignoring for the moment the severe problem of propagating through the stop band, obliquely propagating waves are difficult to reconcile with the conical sheet hypothesis as well as with other observations discussed in Chapter 7. We return to this point in Section 9.4. Nonetheless, in the absence of a detailed comparison between the Weibel and cyclotron mechanisms, it does not appear possible to reach any firm conclusions about the viability of the cyclotron mechanism as the exciter of planetary radio emission.

The loss-cone instability mechanism, taken in a general context to include any instability driven by free energy in perpendicular motion, has several attractive features. For one, in principle it can produce escaping X-mode radiation if it can be shown that growth of the slow mode does not dominate. Loss-cone instabilities are also consistent with Dulk's conical sheet hypothesis, but the other theories also share this property. When combined with models of the global Jovian magnetic field (Chap. 1), this mechanism (as well as others discussed below) provides a possible explanation for the locations of some of the more prominent sources, in particular, sources A and non-Io B [see, for example, Goldstein, Eviatar, and Thieman, 1979; Goldstein and Eviatar, 1979; Oya, Morioka, and Kondo, 1979; Goldstein and Thieman, 1981].

There is a problem, however, with the location of the Io-B source. The origin of this discrepancy could well lie with either the magnetic field models or the emission mechanism. From the analysis by Goldstein, Eviatar, and Thieman [1979] and Goldstein and Thieman [1981], it is clear that neither the Goddard O4 model nor the JPL magnetic field models provide a natural explanation of the Io-B source location within the context of any of the proposed emission mechanisms. In Section 9.4, we return to this problem.

Finally, whereas loss-cone instabilities have of course been invoked to explain observations of TKR, the situation at Jupiter differs in several respects. For example, a satisfactory model of just how Io might drive or enhance a loss-cone process has not been developed.

Summary of direct linear mechanisms

Of the many direct linear mechanisms it is difficult to select one that is the most likely candidate for DAM radiation quite apart from the neglect of nonlinear effects. The properties of the various direct linear mechanisms are summarized in Table 9.1. It appears that processes that generate only the slow X mode must be discarded because of the problem of propagating through the stop zone. The fast X-mode branch will be amplified in the direction of the electron propagation, so that unless the energetic electrons are coming up from the ionosphere, the waves must be reflected before leaving the magnetosphere. The reflection coefficient is certainly less than one, thereby reducing the overall efficiency of the process. The frequency drifts of S-bursts, however, do suggest the possibility of upward propagating electrons (Chap. 7). Any theory that relies on a loss-cone distribution produced by stably trapped particles does not require a downward flux of electrons and hence is not subject to this criticism. However, electrons that reach a 14 G field at the foot of the Io flux tube must be inside the loss-cone. Thus, mechanisms which rely on stably trapped electrons are not applicable to the production of Io controlled DAM.

The highest decameter frequencies can be excited by loss-cone distributions as has been pointed out by Wu and Lee [1979] in their theory of TKR. In their model, precipitating electrons with pitch-angles outside the loss-cone are mirrored so that the albedo distribution shows a depletion near zero pitch angle, that is, the ascending electrons have a loss-conelike distribution. This model has been amplified by Lee, Kan, and Wu [1980] in their paper on TKR. This picture is also a possible candidate for the generation of DAM [Wu and Freund, 1977]. A loss-cone type distribution in the ascending electrons, after mirroring above the ionosphere, could amplify freely escaping quasi-perpendicular fast X-mode waves. Thus, one avoids the problem of reflection alluded to above, but replaces it with another; namely, reduced efficiency because the albedo flux is less than the precipitating flux. As we shall see in the following section, when nonlinear processes are considered, it becomes possible to construct a theory consistent with the conical sheet model without reflecting the particles although still assuming downward propagating beams. This avoids the two losses of efficiency previously discussed. However, the beam driven instabilities require two steps – one to generate electrostatic waves, and a second to up-convert them into fast extraordinary mode waves. This, of course, reduces the overall efficiency of that process. A detailed comparison of the overall efficiencies of loss-cone and beam driven process is yet to be carried out.

The backward propagating ordinary mode in the frequency range $\omega_{ce}/2 < \omega < \omega_{ce}$ requires no reflection and will not encounter a stop band. However, it is elliptically polarized in a LH sense, which is only rarely observed (Chap. 7). Furthermore, as we have pointed out, the growth rates of waves in the ordinary mode are generally less than those of extraordinary waves [Hirshfield and Bekefi, 1963; Lee and Wu, 1980]. At low frequencies (< 1 MHz) the Jovian kilometric radiation (KOM) may well be in the ordinary mode [Warwick et al., 1979b; Green and Gurnett, 1980; Desch and Kaiser, 1980; and Chaps. 7 and 8].

Several of the assumptions made in the derivation of (9.1) impose physical limitations on its application. Interparticle collisions are neglected that could enhance

Table 9.1. *Summary of direct linear mechanisms*

Mode	Frequency range	Direction of propagation	Form of free energy	Comments
Fast x mode		$k_\parallel >> k_\perp$	Excess parallel energy (beams)	Does not produce radiation cones
or x mode or band III	$\omega > \omega_{ce}$	$k_\parallel << k_\perp$	Excess perpendicular energy (loss-cone)	Provides radiation cones. Most commonly assumed linear mechanisms for DAM, HOM
Slow x mode		$k_\parallel >> k_\perp$	Loss-cone (and/or beams)	Whistlers encounters stop zone and cannot escape freely
or z mode or band II	$\omega < \omega_{ce}$	$k_\parallel << k_\perp$	Excess perpendicular energy	Small growth rates Landau damping by thermal particles
Ordinary mode		$k_\parallel << k_\perp$	No resonance possible with electrons	
	$\omega_{ci} < \omega < \omega_{ce}$	$k_\parallel >> k_\perp$	Excess perpendicular energy	Wrong polarization small growth rates, may be responsible for KOM

absorption of electromagnetic waves and would also tend to smooth out velocity-space anisotropies resulting in reduced growth rates. When amplitudes become large, the particle orbit is subject to large deviations from the assumed unperturbed helical trajectory. The linear analysis then must be modified by nonlinear perturbed orbit effects. (For a general discussion of the techniques involved, see Völk [1975].) We have not considered the effects of Landau damping or cyclotron absorption by thermal electrons. Those resonances could quickly damp the slow X mode near the cyclotron frequency. The Landau damping of this (whistler) mode has also been investigated by Menietti and Gurnett [1980] whose results are discussed in Chapter 9.

Indirect emission mechanism

In the previous section, we have seen that an important constraint on the generation mechanisms of DAM radiation is the escape of the radiation. Many linear theories suggest amplification on the slow X branch that cannot escape directly to free space. Oya [1974], Oya, Morioka, and Kondo [1979], Oya, Kondo, and Morioka [1980] have attempted to account for the escape of waves by considering a process which converts the slow extraordinary mode into the escaping ordinary mode. The coupling is found to be especially strong in the vicinity of the point where the wave frequency equals the local plasma frequency (ω_{pe}). The extraordinary mode is obtained as a result of mode coupling between a beam excited upper-hybrid resonance electrostatic wave and plasma inhomogeneities [Zheleznyakov, 1966]. Apart from the severe difficulties inherent in proposing a mechanism whose overall efficiency is proportional to the product of three processes, all of which with intrinsic efficiencies less than one (beam to electrostatic, electrostatic to X mode, and X mode to O mode), Oya's theory requires plasma densities in excess of 10^7 cm^{-3} to meet the condition $\omega = \omega_{pe}$. In the Jovian ionosphere, the maximum plasma frequency is no greater than about 3 MHz (Chap.2). Futhermore, the resulting O-mode radiation requires that the DAM sources lie primarily in the southern hemisphere. This appears contrary to the Voyager observations described in Chapter 7.

We now turn to an investigation of beam-driven instabilities. We will find that some of the difficulties experienced by loss-cone driven processes are absent, only to be replaced by new problems that we have not as yet discussed.

9.3. Nonlinear theories

Indirect emission mechanisms

We have seen that many attempts at explaining the Jovian decameter radiation involve direct excitation of electromagnetic radiation by energetic electrons. Several examples of such theories have been discussed. Common to those theories is the assumption that the energetic electron distribution function contains more free energy in velocity components perpendicular to the magnetic field than parallel to it as is the case for electromagnetic instabilities driven by loss-cone distributions or temperature anisotropies with $T_\perp > T_\parallel$. It is clear from the discussion in Section 9.2 that none of these theories is without its difficulties in accounting for the rich phenomenology of DAM. Recently, it has been suggested that the decameter radiation can arise from indirect processes where the energetic electrons first excite electrostatic waves ($E = E_\parallel$), which then combine to produce the observed electromagnetic radiation. To some extent these theories are motivated by similar analyses of TKR.

The indirect emission mechanisms start with the assumption that the distribution function of energetic electrons is essentially that of a beam; the excess free energy is parallel to the magnetic field. This is precisely the complement of the examples discussed in Section 9.2.

Application of indirect nonlinear emission mechanisms to the problem of generating DAM has occurred only fairly recently. Earlier, mode coupling theories have been proposed for generation of type III (fast drift) solar radio bursts [Papadopoulos, Goldstein, and Smith, 1974], and generation of TKR [Barbosa, 1976; Maggs, 1978; Roux and Pellat, 1979]. In their 1979 paper, Roux and Pellat suggested that their up-conversion process for the generation of TKR might be adaptable to the Jovian problem. They noted that beam driven instabilities could excite both upper-hybrid and lower-hybrid waves that in turn could couple to produce electromagnetic radiation. In the terrestrial environment, they had concluded that the most appropriate coupling would result in either an ordinary mode wave near ω_{UHR}, or an extraordinary mode wave at $2\,\omega_{UHR}$ (for a related analysis see Barbosa [1976]). However, in the Jovian magnetosphere, where $\omega_{pe}/\omega_{ce} << 1$, Roux and Pellat recognized that the coupling $\omega \gtrsim \omega_{LHR} + \omega_{UHR}$ might produce radiation above ω_R, the right-hand cut-off frequency defined following (9.7); thus giving a freely escaping electromagnetic wave with frequency close to the local gyrofrequency.

Detailed analyses of several nonlinear indirect mechanisms for the production of DAM, including the possibility suggested by Roux and Pellat [1979], have been developed recently. The first is the work of Ben-Ari [1980] who assumed that a beam of electrons was accelerated by the motion of Io (see discussion in Section 9.4). In the source region the density of the beam n_b was assumed less than n_e, in contrast to some of the theories of TKR described above in Section 9.2 . Because the plasma is characterized by $\omega_{ce} >> \omega_{pe}$, such a "bump-in-tail" distribution is unstable to the excitation of upper-hybrid electrostatic waves. Ben-Ari considered four different resonant three wave interactions that could couple upper-hybrid waves to electromagnetic radiation above ω_R. In a subsequent paper, Goldstein et al. [1982] included the excitation of lower-hybrid waves by the same electron beam and then analyzed the up-conversion of upper-hybrid and lower-hybrid waves in detail.

We first briefly review some aspects of these up-conversion theories. For the purposes of this discussion, we assume the existence of a beam of energetic electrons in the Jovian magnetosphere. In Section 9.4 we discuss a possible way to produce beamlike distributions, but here we proceed without any consideration of the beam generation mechanism and merely explore the consequences of this assumption.

Let $F_e(v_\parallel, v_\perp)$ be the total electron distribution function made up of a cold thermal component (0.1 eV thermal energy), and an energetic beam. It suffices in describing the linear electrostatic instability to approximate the electron motion perpendicular to the magnetic field as cold. Thus, we take $F_e(v_\parallel, v_\perp) = F_e(v_\parallel)\,\delta(v_\perp) / 2\pi v_\perp$, with $F_e(v_\parallel) = f_e(v_\parallel + (n_b / n_e) f_b(v_\parallel)$. The thermal component with density n_e and the beam with density n_b have distributions denoted by f_e, and f_b, respectively. We represent each with a Maxwellian, so that

$$f_e(v_\parallel) = \frac{1}{(2\pi)^{1/2} V_e} \exp\left[- \frac{v_\parallel^2}{2 V_e^2} \right] \tag{9.9}$$

$$f_b(v_\parallel) = \frac{1}{(2\pi)^{1/2} V_b} \exp\left[- \frac{(v_\parallel - u)^2}{2 V_b^2} \right]$$

where V_e is the thermal velocity, V_b the thermal spread of the beam, and u the beam speed. The phase velocities of the upper-hybrid and lower-hybrid waves can be calculated from the real part of the cold-plasma dielectric function [Harris, 1968]

$$\epsilon = 1 - \omega_{pe}^2 \left(\frac{\sin^2\theta}{\omega^2 - \omega_{ce}^2} + \frac{\cos^2\theta}{\omega^2} \right) - \frac{\omega_{pi}^2 \sin^2\theta}{\omega_{ci}^2} \tag{9.10}$$

where θ is the angle between **k** and **B**.

The solution for the high frequency branch (between the electron cyclotron frequency and the upper-hybrid frequency, is

$$\omega^2 = (1/2)\left[\omega_{UHR}^2 + (\omega_{UHR}^4 - 4\omega_{ce}^2\omega_{pe}^2\cos^2\theta)^{1/2}\right] \tag{9.11}$$

The frequency of this mode ranges between ω_{ce} at $\theta = 0$ and ω_{UHR} at $\omega = \pi/2$. The low frequency mode is given approximately by

$$\omega_l^2 \simeq \omega_{pe}^2\cos^2\theta + \omega_{pi}^2 \tag{9.12}$$

The growth rate for these electrostatic waves can be found from (9.1) or (A.24) if the electrostatic term proportional to $E_\parallel$ is the only one retained and the nonrelativistic approximation is made. Thus from (9.1),

$$\gamma = -\frac{4\pi^2 e^2 n_e}{m_e k^2} \sum_\nu \int_0^\infty 2\pi v_\perp dv_\perp J_\nu\left(\frac{k_\perp v_\perp}{\omega_{ce}}\right) \tag{9.13}$$

$$\times \left[\left(\frac{\partial}{\partial v_\parallel} + \frac{\nu\omega_{ce}}{k_\parallel v_\perp}\frac{\partial}{\partial v_\perp}\right) F_e(v_\parallel, v_\perp)\Big|_{v_\parallel = (\omega - \nu\omega_{ce})/k_\parallel}\right] / (\partial\epsilon/\partial\omega)$$

the only important contributions in (9.13) come from the $\nu = 0$ and $\nu = -1$ terms [Goldstein et al., 1982]. If the thermal plasma is assumed sufficiently cold, the contributions from the ambient electrons can be neglected and γ reduces to

$$\gamma = \tag{9.14}$$

$$\left(\frac{\pi}{2}\right)^{1/2}\left(\frac{\omega}{2k^2}\right)\left\{\frac{n_b(u - \omega/k_\parallel)}{n_e V_b^3}\exp - \frac{(\omega/k_\parallel - u)^2}{2V_b^2} + \frac{k_\perp^2}{k_\parallel\omega_{ce}}\frac{n_b}{n_e} f_b\left(\frac{\omega + \omega_{ce}}{k_\parallel}\right)\right\}$$

$$\left[\frac{\omega^2\sin^2\theta}{(\omega^2 - \omega_{ce}^2)^2} + \frac{\cos^2\theta}{\omega^2} + \frac{\omega_{pi}^2\omega^2\sin^2\theta}{\omega_{pe}^2(\omega^2 - \omega_{ci}^2)^2}\right]$$

where the first term in the denominator represents the interaction of the plasma and beam and the last term represents the anomalous ($\nu = -1$) Doppler contribution from the beam.

The high frequency wave will be excited through the beam-driven Landau resonance with growth rate

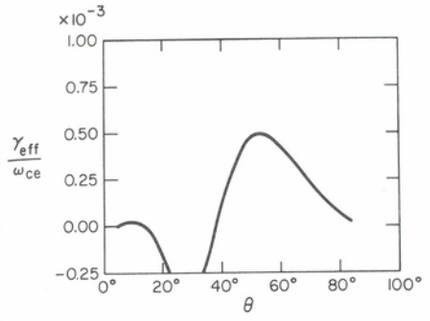

Fig. 9.3*a*. Growth rate of the upper-hybrid wave as a function of angle of propagation for $\omega_{pe}/\omega_{ce} = 0.1$. Cyclotron damping is included.

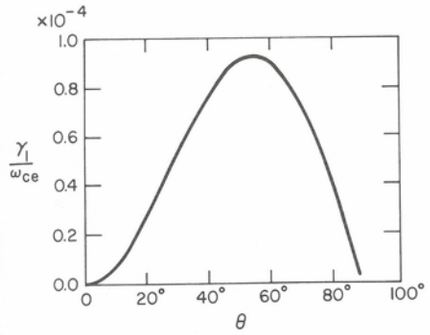

Fig. 9.3*b*. Similar to Figure 9.3*a*, but for the lower-hybrid wave.

$$\gamma = \left(\frac{\pi}{2}\right)^{1/2}\frac{n_b}{n_e}\frac{\omega_{ce}}{2}\left(\frac{\omega_{pe}}{\omega_{ce}}\right)^4\left(\frac{u}{V_b}\right)^2\cos^2\theta\sin^2\theta \tag{9.15}$$

$$\times\left(\frac{u}{V_b} - \frac{\omega_{ce}}{kV_b\cos\theta}\right)\exp\left[-(u - \omega_{ce}/k\cos\theta)^2/2V_b^2\right]$$

Similarly the growth rate of the low-frequency wave, driven unstable by the cyclotron term is

$$\gamma_l \simeq \frac{\omega_{pe}}{8}\left(\frac{\omega_{pe}}{\omega_{ce}}\right)^2\left(\frac{u}{V_b}\right)\sin\theta\sin 2\theta\left(\frac{n_b}{n_e}\right)\exp\left[-\frac{(\omega_{ce} - k_l u\cos\theta)^2}{2V_b^2 k_l^2\cos^2\theta}\right] \tag{9.16}$$

where we have assumed that θ is not too close to $\pi/2$ so that the ion terms can be neglected. Note that for both upper-hybrid and lower-hybrid waves, $k \simeq \omega_{ce}/u\cos\theta$.

In Figure 9.3, taken from Goldstein et al. [1982], we plot the magnitude of these growth rates for $n_b/n_e \simeq 10^{-2}$ and $\omega_{pe}/\omega_{ce} = 0.1$. Both γ and γ_l peak for propagation near 50°, which is consistent with the claim made in Section 9.2 that beam driven instabilities tend to excite obliquely propagating waves. The choice of 10^{-2} for n_b/n_e is made solely for illustrative purposes as it is by no means certain that any of the energetic electron populations that have been observed in the Jovian magnetosphere are the exciters of DAM, (see Chaps. 5 and 12). The source for the DAM is intimately associated with the current system driven by the motion of Io through the plasma torus, and there have been no in situ observations of the electron distribution function inside

the current carrying flux tube. In 9.3*a* cyclotron damping by the thermal plasma has been included. For a detailed discussion of its importance the reader is referred to Goldstein et al. [1982].

Three-wave interactions

The electrostatic waves excited by the beam must be converted into electromagnetic wave modes in order to produce the observed decameter radiation. There are several possibilities. We confine our attention to three-wave processes that can become important if the intensity of the upper-hybrid wave grows to a large amplitude. One possibility is that an intense upper-hybrid wave can decay into two other waves, one of them electromagnetic. That process can be schematically denoted.

$$\sigma \rightarrow \sigma_1 + \sigma_2 \tag{9.17}$$

This notation implies that two resonance conditions must be satisfied, one requiring momentum conservation:

$$\mathbf{k} = \mathbf{k}_1 + \mathbf{k}_2$$

and a second ensuring conservation of energy (frequency matching):

$$\omega = \omega_1 + \omega_2$$

Alternatively, the upper-hybrid wave could combine with a second electrostatic wave to produce an electromagnetic wave. This process is known as up-conversion, which we denote as

$$\sigma + \sigma_1 \rightarrow \sigma_2 \tag{9.18}$$

The resonance conditions become

$$\mathbf{k} + \mathbf{k}_1 = \mathbf{k}_2 \qquad \text{and} \qquad \omega + \omega_1 = \omega_2$$

Decay instabilities

Ben-Ari [1980] has considered decay interactions in which the σ_1 wave was either a lower-hybrid wave, an ion cyclotron wave, or an ion acoustic wave. She showed that when an upper-hybrid wave decays into a lower-hybrid wave, the resulting electromagnetic wave will be either an ordinary mode wave propagating across the field, or an extraordinary mode wave propagating along the field, antiparallel to the direction of the beam. Alternatively, if the decay produces a low frequency electrostatic ion cyclotron wave, then the resonance conditions restrict the electromagnetic wave to only the ordinary mode. Furthermore, decay into electrostatic ion cyclotron waves is unlikely because a higher threshold is required than for decay into a lower-hybrid electrostatic wave. Another possibility is that the decay product can be an acoustic wave. This can only happen if the thermal electron temperature exceeds the thermal ion temperature by an amount sufficient to allow ion acoustic waves to propagate as a normal mode of the plasma [see Krall and Trivelpiece, 1973]. Ben-Ari found that the largest decay rates produced ordinary mode electromagnetic waves in the direction antiparallel to the beam direction.

From these results it appears unlikely that decay instabilities (9.17) play a dominant role in exciting DAM, primarily because DAM appears to be almost entirely extraordinary mode radiation. The one possibility that can generate extraordinary mode radiation requires that the radiation be emitted along the field. In Section 9.2 we discussed the difficulties associated with parallel propagation. This leaves up-conversion as the most promising nonlinear process. We now consider the up-conversion of a lower-hybrid and upper-hybrid wave in greater detail.

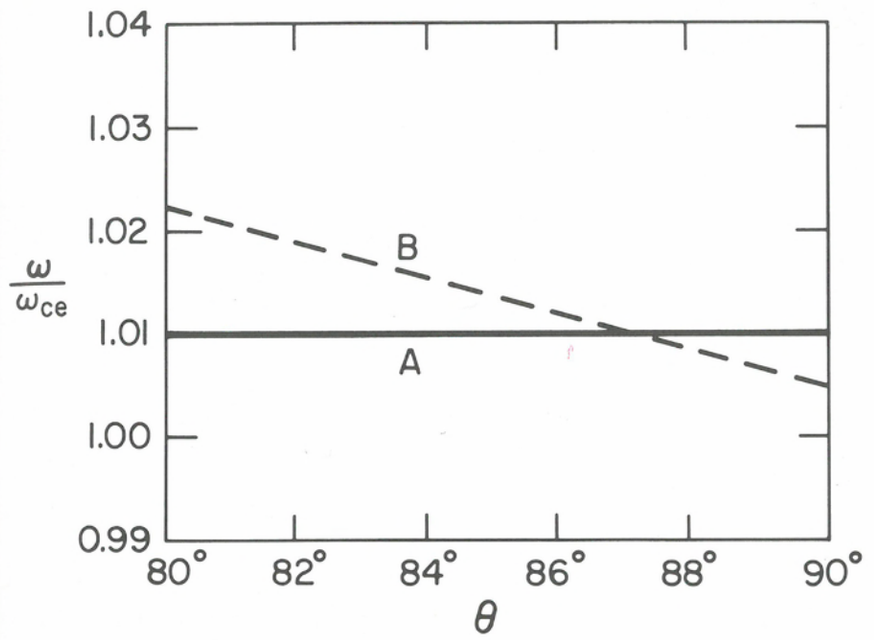

Fig. 9.4. The right-hand cutoff frequency ω_R (curve A) and the upconverted frequency ω (curve B) are shown as functions of θ, the propagation angle. Up-conversion is possible only for angles of propagation for which $\omega > \omega_R$.

Three-wave up-conversion

The frequency matching condition requires that the frequency of the up-converted wave, given by $\omega_2 = \omega + \omega_1$, must be greater than ω_R. The constraints under which this can be satisfied are illustrated in Figure 9.4. Assuming that $\omega_{pe}/\omega_{ce} \simeq 0.1$, ω_2 can exceed ω_R if θ, the angle between **B** and **k** is less than about 88° (implicit in Figure 9.4 is the assumption that θ for both electrostatic waves has the same magnitude). Recall that the growth rates for the lower-hybrid and upper-hybrid waves were greatest near 50°, thus up-conversion is apparently allowed. Ben-Ari [1980] considered this regime and found that the up-converted waves preferentially propagated nearly parallel to **B**. Thus, if one wishes to produce a hollow conical emission pattern, up-conversion cannot take place in the same physical location as the excitation. This has led Goldstein et al. [1982] to reconsider the up-conversion process by allowing for the possibility that once amplified the electrostatic waves propagate and refract so that the conversion to electromagnetic radiation will not occur where the electrostatic waves are first produced [cf., Roux and Pellat, 1979]. In addition, Goldstein et al. assume that the lower-hybrid waves are self-consistently amplified by the same electrons that excite the upper-hybrid waves.

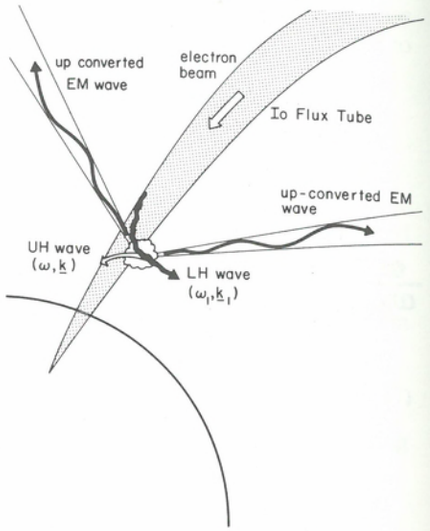

Fig. 9.5. A schematic view of the excitation, propagation, and refraction of electrostatic lower-hybrid and upper-hybrid electrostatic waves. Up-conversion would produce a hollow conical emission pattern of fast X mode radiation.

Because the wave number of the electromagnetic wave is small, that is, $|\mathbf{k}_2| << |\mathbf{k}|$ or $|\mathbf{k}_1|$, the three-wave resonance for up-conversion requires that $\mathbf{k} \simeq -\mathbf{k}_1$. Consequently, the two electrostatic waves must propagate in opposite directions for the up-conversion to take place. As we have seen, an electron beam is unstable to excitation of both upper-hybrid waves and lower-hybrid waves. If the high frequency wave is excited by the Landau resonance (see Eq. 9.15), and the low frequency wave is excited by the cyclotron resonance (Eq. 9.16), then one is guaranteed that $|\mathbf{k}| \simeq |\mathbf{k}_1| \simeq \omega_{ce}/u \cos\theta$.

Both waves have phase velocities close to the velocity of the beam. However, although the low frequency wave also propagates with a group velocity whose parallel component is in the beam direction, the parallel component of the group velocity of the high frequency wave is antiparallel to the beam. The vector direction of the group velocity of each of the waves is orthogonal to its phase velocity [Stix, 1962].

As the group velocity of the high frequency wave propagates upward, the wave encounters a region where the frequency equals the local upper-hybrid frequency. From (9.10) and (9.11) it is clear that as $\omega \to \omega_{UHR}$, $\theta \to \pi/2$. The group velocity approaches zero at this resonance. On the other hand, the low frequency wave encounters the ion plasma frequency as it propagates downward into higher density regions (cf., Eq. 9.12). The phase velocity of this wave also refracts toward $\pi/2$ and the group velocity again approaches zero. As a result the two waves can have oppositely directed wave vectors as required by the resonance condition. This model requires that although the upper- and lower-hybrid waves are both generated by the electron beam, the waves are not generated in the same place. This is schematically illustrated in Figure 9.5. As long as the wave-particle resonance conditions are satisfied during the refraction, the electrostatic waves will experience a convective amplification.

Recall from Figure 9.4 that frequency matching requires that $\theta < 88°$. A quantitative estimate of how close to $\pi/2$ the electrostatic waves must be to satisfy the wave-number matching condition (9.18) is also necessary. Because the perpendicular components of $\mathbf{k}$ are conserved during propagation of the electrostatic waves, $\mathbf{k}_\perp + \mathbf{k}_{1\perp} \simeq 0 \simeq \mathbf{k}_{2\perp}$ so long as the density gradients in the source region are much greater than the gradients in $\mathbf{B}$. However, both electrostatic waves have parallel

components of their wave vectors in the same direction so that $k_\parallel + k_{1\parallel} \simeq 2k_\parallel$. Up-conversion to an electromagnetic wave propagating nearly orthogonal to $\mathbf{B}$ then requires that

$$2k_\parallel = k_{2\parallel} << k_{2\perp} = k_2 \sin\theta_2 \tag{9.19}$$

An estimate of $k_{2\parallel}$ can be obtained by noting that close to the reflection point the amplitudes of the electrostatic waves are described by Airy functions [Ginzburg, 1970; Roux and Pellat, 1979]. The wavelength in the vicinity of the reflection point is approximately the distance from the point of reflection to the first maximum of the Airy function, or

$$k_\parallel \simeq 2\pi (k_{0\parallel} L_N)^{2/3}/L_N \tag{9.20}$$

where L_N is the density scale height at the point of reflection and $k_{0\parallel}$ is the initial magnitude of the parallel component of $\mathbf{k}$ or $\mathbf{k}_1$ at the point of excitation, that is, $k_0 \simeq \omega_{ce}/u \cos(50°)$. The density scale height is estimated to range from 600–900 km in the Jovian ionosphere (see Chap. 2). This implies from (9.19) and (9.20) that $\theta_2 \gtrsim 50°$ for 20 MHz radiation. Taken together with the frequency matching requirement that $\theta \lesssim 88°$, we see that the up-conversion process can generate fast X-mode radiation in a hollow conical emission pattern.

The model described above requires a single electron beam directed downward. In Section 9.4 we describe a model of the coupling between Io and energetic electrons that produces two electron beams; one directed downward and the second directed upward. The two beams are on opposite sides of the Io flux tube. This suggests the possibility that the electrostatic waves could propagate across the flux tube with relatively little refraction and then up-convert. In that case the parallel components of the wave vectors would be oppositely directed and the constraints on the wave-number matching would be even less severe. Whether this geometry would result in a hollow conical emission pattern has not as yet been worked out.

We have so far shown that electron beams can excite electrostatic waves, that these waves can propagate to a geometrical configuration where the three-wave up-conversion matching conditions can be met, and that the resulting electromagnetic radiation will be beamed into a hollow conical emission pattern (see Fig. 9.5). Up-conversion processes can be intrinsically inefficient and it is important to estimate the coupling coefficients and the energy requirements before concluding that the process is viable. Roux and Pellat [1979] have computed the coupling of a coherent three-wave interaction involving two upper-hybrid waves. The coupling efficiency of an upper- and lower-hybrid wave has been computed by Goldstein et al. [1982] who considered only the coupling of incoherent waves. The derivation of the coupling coefficients is a very lengthy exercise that we will not repeat. Rather, we limit ourselves to a discussion of the underlying physics and discuss some of the results. The interested reader is referred to Davidson [1972] and Tsytovich [1970] for more details. The full generalization to electromagnetic waves can be found in Pustovalov and Silin [1975], and Larson and Stenflo [1976]. The application to TKR was discussed by Barbosa [1976] and Roux and Pellat [1979], and application to DAM by Ben-Ari [1980] and Goldstein et al. [1982].

The nonlinear currents that generate the up-converted electromagnetic wave can be computed if one uses fluid equations to describe the motion of the electrons in response to both the electrostatic fields and the magnetic fields. One approach is to linearize the electron fluid equations for conservation of electron mass and momentum. One of the contributions to the nonlinear current can be computed from the terms representing

the product of the electron density perturbations driven by the upper-hybrid wave and the electron velocity perturbations driven by the lower-hybrid wave. In a similar manner, the lower-hybrid density fluctuations and the upper-hybrid velocity perturbations produce a second term in the nonlinear current. A third contribution comes from the pondermotive force that arises from the interaction of the perturbation velocities of the upper- and lower-hybrid waves through the $(\mathbf{v}\cdot\nabla)\mathbf{v}$ term in the momentum equation. The resulting force produces a nonlinear velocity perturbation v_{NL}. The current can then be written [Goldstein et al., 1982]

$$J_{NL} = -ne\mathbf{v}_l/2 - n_l e\mathbf{v}/2 - n_e e\mathbf{v}_{NL} \tag{9.21}$$

This current then enters the right-hand side of Equation (A.1), where now Λ_{ij} and E_j describe the cold plasma dispersion relation and electric field of the up-converted electromagnetic wave. From (9.21) and (A.2), one can derive an equation relating the amplitude of the electromagnetic wave to the product of the amplitudes of the two electrostatic waves. Details can be found in the papers referenced above.

The efficiency of this process can be estimated by asking what fraction of the energy in the beam must be converted into electrostatic energy to produce the observed power in decameter radiation. Such an estimate has been made for the incoherent process described by Goldstein et al. [1982]. They found that the observed radiation could be accounted for if approximately 10^{-3}–10^{-4} of the beam energy was converted into electrostatic waves. These estimates depend on the choice made for the source size, ambient electron density, beam density, etc., and the reader is referred to their paper for more details. Their calculation ignores the geometric amplification of the electrostatic waves known to occur near resonance. This amplification can be estimated from knowledge of the Airy functions mentioned above and has been done by Roux and Pellat [1979] for the upper-hybrid wave in the terrestrial magnetosphere. Computer simulations of the electrostatic simulations described above have shown that as much as 10% of the beam energy can be converted into electrostatic waves [Rowland, Palmadesso, and Papadopoulos, 1981]. Thus, the indirect up-conversion process appears to be a viable candidate for producing DAM.

Direct emission mechanisms

Although we have discussed what must appear to be a plethora of emission mechanisms for exciting the DAM, we have by no means exhausted all of the possibilities considered in the literature. In addition to the indirect wave coupling process described above where the beam first excites two electrostatic waves that in turn up-convert to give the escaping electromagnetic radiation, one can imagine situations where the beam directly amplifies fast X-mode electromagnetic radiation via a direct coupling with a second intense electrostatic wave. Two theories have been proposed for TKR based on this approach. Neither has been applied to the Jovian situation, primarily because it is not clear that the high efficiencies obtained in these direct mode coupling theories are required by the observed emission. In addition, one also would need to assume the existence of some source of intense, coherent, electrostatic waves. Although these have been observed in the Earth's auroral zone, they have not been reported at Jupiter. Of course, such waves would not propagate from the region of excitation, and so would be confined to the presumed DAM source region in the upper ionosphere.

The first of these two direct nonlinear theories [Palmadesso et al., 1976] assumed the existence of electrostatic electron cyclotron waves. For efficient coupling, the

escaping electromagnetic wave then had to be in the O mode. Subsequently, Grabbe, Papadopoulos, and Palmadesso [1980] and Grabbe [1981b], motivated by observations of large amplitude coherent electrostatic ion cyclotron (EIC) waves in the auroral zone [see, e.g., Lysak, Hudson, and Temerin, 1981], assumed that the electrostatic waves were EIC. In these papers, the authors showed that interaction between EIC waves and the electron beam could produce escaping fast X-mode radiation just above ω_R in a source region with $\omega_{pe} < \omega_{ce}$. We will not describe these theories here in any greater detail. The interested reader will find more complete descriptions in the references cited above and in a review of TKR theories by Grabbe [1981a].

In the nonlinear theories discussed above, the existence of an electron beam is required. Because it is believed that most DAM is controlled in some way by Io, we are faced with the question of how Io can produce an electron beam. Details of the interaction of Io with the corotating plasma are described in Chapter 10. In the next section we discuss those aspects of this interaction that bear on the generation of electron beams. We also discuss a few aspects of DAM morphology related to this same "coupling mechanism" [Smith, 1976a].

9.4. The Io and plasma torus interaction

Since the discovery by Bigg [1964] of the remarkable control of the orbital position of Io over the DAM radiation, considerable theoretical attention has been given to the explanation of the Io interaction with the Jovian magnetosphere. Several mechanisms including the excitation of large amplitude MHD waves, the generation of electrostatic electric fields parallel to **B** and the effects of the Io wake have been considered. The recent Voyager 1 and 2 encounters have altered our view of the basic Io interaction considerably. The plasma environment of Io is quite different from what had been assumed earlier and the great Io torus affects significantly the interaction of Io with the magnetosphere (Chap. 10). It also changes the propagation characteristics of electromagnetic waves and determines much of the phenomenology and morphology of KOM radiation (see Chap. 7).

In this section we review one mechanism by which Io can accelerate electrons. The end result is an electron distribution that satisfies the requirements discussed in Section 9.3 for beam-driven instabilities. However, because loss-cone distributions may arise from beamlike distributions after magnetic mirroring, we cannot use the Io-magnetosphere coupling mechanism described below to choose indirect over direct emission mechanisms with certainty, although the model is suggestive that beamlike distributions should arise relatively naturally.

Generation of Alfvén waves by Io

The interaction of Io with the corotating torus plasma is described in Chapter 10. It seems that Io's interaction is electromagnetic in nature and related to the induced electric field on Io moving through the magnetized plasma [Neubauer, 1980]. This field drives an electric current through Io (either through its body or through its ionosphere), which produces polarization perturbations of the electric field and these are transferred to the plasma along magnetic field lines. As a result, the plasma velocity in Io's vicinity changes. Far away from Io the plasma corotates at a velocity $v_0 = \omega r$. Near Io the plasma is slowed down to $v_{Io} = v_0 - v_\perp$. The velocity perturbation $v_\perp = v_0 - v_{Io}$ is discussed in Chapter 10. A schematic view of the situation is shown

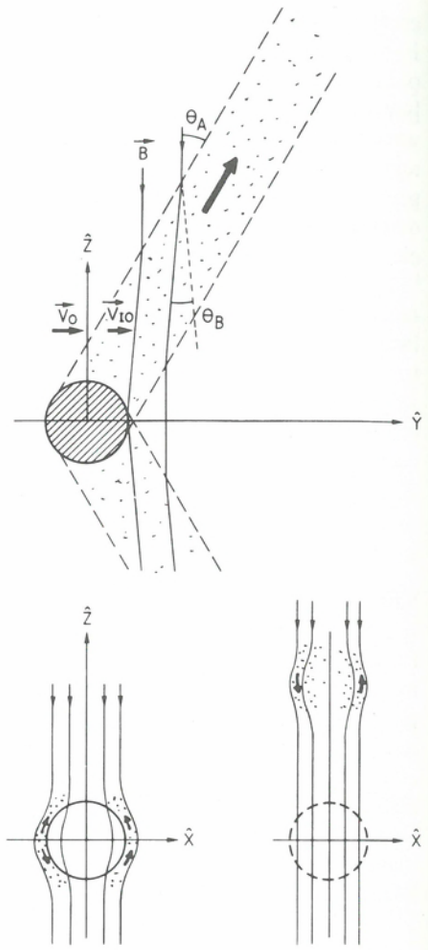

Fig. 9.6. A sketch of the Alfvén wave model for the Io interaction as seen in Io's frame. The top figure shows the Alfvén wings as dashed lines and the magnetic field lines as solid lines. The bottom two figures show the magnetic field configurations in the $\hat{x}$–$\hat{y}$ plane at different values of $\hat{y}$. $\hat{y}$ is the direction of the torus plasma flow relative to Io. The acceleration of electrons takes place at the Alfvén wings and the space between the wings is filled with accelerated electrons, represented by the dots. These electrons carry a current parallel to the Alfvén wings, indicated by the heavy arrows. The reduction of the plasma convection velocity behind the Alfvén wings is also indicated. The reader is referred to Chapter 10 for more details.

in Figure 9.6. Io interacts with the plasma through what has been called an "inductive interaction" [Gurevich, Krylov, and Fedorov, 1978] by which magnetohydrodynamic waves are produced. The circuit for the current flowing through Io is closed in the plasma by currents flowing in the wave fronts. Note that the waves are not harmonic waves, but comprise a pulselike wave packet. Direct measurements of the perturbation magnetic fields produced by this current system have been reported by Acuña, Neubauer, and Ness [1981]. The only mode that can guide energy along the field lines is the Alfvén wave. Hence, it alone can account for a small source size near the Jovian ionosphere of the Io controlled DAM. The other two MHD modes are not guided and will not be considered here. Under certain conditions, for example, low plasma density and small scale sizes, the field aligned currents in the Alfvén wave are carried by accelerated electrons, i.e., a beam. The energy of these electrons can be estimated from the properties of the electric field of the Alfvén wave.

The Alfvén waves created by Io are shear Alfvén waves. Because the disturbance is spatially localized, one must view it as a wave packet consisting of a Fourier spectrum in the perpendicular wave-number $k_\perp$. The Fourier components of this shear Alfvén wave propagate obliquely with respect to the background magnetic field $\mathbf{B}_0$ although

the wave packet itself propagates almost exactly along the field lines in Jupiter's frame of reference. (The group velocity of Alfvén waves is along **B**.) The "quality" of guidance of the wave-packet along the magnetic field depends on two factors: The amount of dispersion and dispersive spreading of the wave packet and, the inhomogeneities of the medium where the wave propagates. The fact that for $k_\perp \neq 0$ Alfvén waves are dispersive is a well documented but little known fact [see, e.g., Fejer and Lee, 1967]. Due to the dispersive nature of obliquely propagating Alfvén waves, a wave packet will spread out as it propagates. The spread is rapid for large values of $k_\perp$ and slow for small values; a critical wave number above which dispersion is strong is ω_{pe}/c for a cold plasma ($\beta < m_e/m_i$) and ω_{ci}/V_i for a warm plasma ($1 > \beta > m_e/m_i$). In the center of the Io torus $T_i \simeq 20$ eV, $n \simeq 2 \times 10^3$ electrons/cm^3, $B_0 \simeq 2 \times 0^{-2}$ G, and $\beta \simeq 4 \times 10^{-3}$. But because β rapidly decreases along a field line as the wave propagates away from the torus, we need consider only the cold plasma case. This situation has been treated by Fejer and Lee [1967], and the reader is referred to that paper for more details. Fejer and Lee also consider the effect of inhomogeneities, and show that unless there are strong perpendicular density gradients, geometrical guiding by the magnetic field is maintained and $k_\perp B =$ constant. Without dispersion the Io created perturbation would thus remain confined to the IFT.

The perturbation created by Io has a rather complicated structure perpendicular to $\mathbf{B}_0$ [Goertz, 1980a] and it is difficult to evaluate the dispersive spreading. Goertz describes the electric field perturbation as consisting of a uniform field $E_\perp$ inside the Io flux tube and a "dipolar" component outside (as seen from Jupiter). The boundary across which $E_\perp$ changes rapidly from dipolar to uniform is assumed to have a thickness d_0 of roughly one (Io) ionospheric scale height (~ 80 km) (see Chap. 3). It can be shown that as the packet propagates along **B**, dispersion will cause this transition region to broaden to an equivalent width w, where

$$w^2 \simeq d^2(1 + 4z^2\omega^2c^4/V_A^2\omega_{pe}^4\pi d^4) = d^2(1 + z^2/z_0^2) \tag{9.22}$$

where $d = d_0B_0/B$ is the thickness one would obtain without dispersion, z is distance along the field line, ω is a characteristic frequency of the wave packet related to the duration T that a field line is in contact with Io by $\omega \simeq \pi/T$. For a weak perturbation, T is the convection time past Io (about 60 s). However, in Chapter 10 it is argued that near Io the electric field is reduced by at least a factor of three and the duration is hence increased to at least 180 s. In the center of the torus the "dispersion length" z_0 is larger than 10^6 R_J and broadening of the transition due to dispersion should be entirely negligible in the torus. At high latitudes along the Io flux tube, dispersion can also be ignored. Therefore, in the following discussion, we assume that the transition from a dipolar electric field outside of the IFT to a uniform $E_\perp$ inside the IFT occurs over a width equal to d.

Alfvén waves generated by Io carry a field aligned current that flows in the transition region where $E_\perp$ changes. This current is carried by electrons that are accelerated by the field aligned electric field. The magnitude of this field can be estimated from either a guiding center Vlasov equation [Fejer and Kan, 1969] or a fluid model [Goertz and Boswell, 1979]. The electric field component $E_\parallel$ in the advancing wave front is related to the perpendicular electric field amplitude $E_\perp$ by

$$E_\parallel = \frac{m_e}{m_i}\,\frac{c}{\omega_{pi}\,\omega_{ci}}\,\frac{d}{dt}\,\nabla \cdot (\mathbf{E} \times \mathbf{B}/B) \tag{9.23}$$

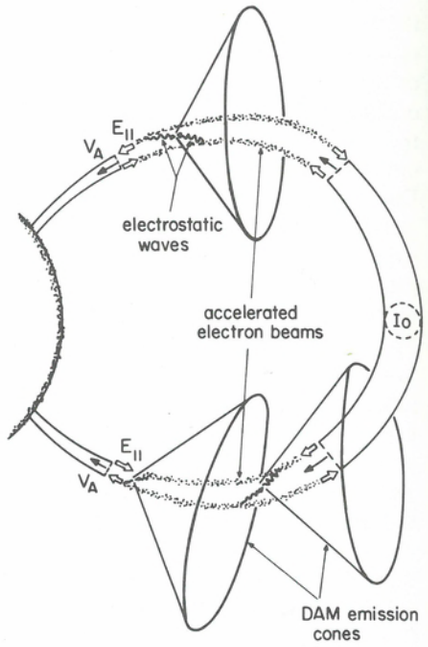

Fig. 9.7. The emission geometry for the Io-phase control of DAM. At the leading and trailing edges of the Io-generated Alfvén wave packet, parallel electric fields accelerate and decelerate electrons. The electrons then form beams between the leading and trailing fronts. In this model, these beams then generate electrostatic waves that in turn couple and up-convert to DAM as described in Section 9.3.

Electrons overtaken by the wave will be accelerated and gain parallel momentum (recall that $\beta < m_e/m_i$ corresponds to $V_A^2 > k_B T_e/m_e$

$$\Delta p_\parallel = \int dt\, qE_\parallel = \frac{m_e}{m_i}\frac{c}{\omega_{pi}}\frac{q}{\omega_{ci}}\nabla\cdot(\mathbf{E}\times\mathbf{B}/B) \simeq \frac{m_e}{m_i}\frac{c}{\omega_{pi}}\frac{q}{\omega_{ci}}\frac{E_\perp}{d} \tag{9.24}$$

An electron will then gain an amount of energy parallel to B_0 equal to

$$\Delta W_{\parallel e} = \Delta p_\parallel^2/2m_e = \frac{c^2}{\omega_{pe}^2 d^2}\frac{m_i}{2}\left(c\frac{E_\perp}{B_0}\right)^2 \tag{9.25}$$

Because of their larger mass, ions gain a much smaller amount of parallel energy. They do, however, gain perpendicular energy as they are overtaken by the wave. In Chapter 10 it is shown that $E_\perp$ near Io can be comparable to the corotational field and hence $\Delta W_{\parallel e}$ can be of the order of several keV at high latitudes.

These considerations suggest the following schematic model for the generation of DAM which is illustrated in Figure 9.7. Between the leading and trailing edge of the Alfvén wave packet, accelerated electrons exist with energies of several keV. The electrons form two beamlike distributions. The beams on the inner and outer sides of the flux tube consist of electrons streaming toward and away from the ionosphere, respectively. As we have seen in Section 9.3, both beams will be unstable against the growth of electrostatic waves propagating antiparallel to each other albeit on opposite sides of the IFT. If these waves propagate across the flux tube, up-conversion may occur, but in any event up-conversion can take place as the waves refract near the resonance layers as described in Section 9.3. The efficiency of such a model and its relation of DAM morphology needs to be investigated in greater detail.

Relation to DAM morphology

Recently there has been considerable interest in calculating what a distant observer will see if the emission pattern is indeed that of a conical sheet [Warwick et al., 1979b; Goldstein and Theiman, 1981; Pearce, 1981; Staelin, 1981; Warwick, 1981]. The problem is essentially that of computing the intersection of a cone with a plane. The axis of the cone is aligned with the direction of the local magnetic field. The plane contains the observer and is usually assumed coincident with, or parallel to, the equatorial plane of Jupiter. The intersection of a conical sheet with a plane is a hyperbola and the angle between the asymptotes of this hyperbola is 2μ where [Goldreich and Lynden-Bell, 1969]

$$\tan\mu = (\tan^2\psi\cos^2\iota - \sin^2\iota)^{1/2} \tag{9.26}$$

In (9.26), ψ is the half angle of the cone, and ι measures the inclination of the axis of the cone to the plane. It is related to $\mathbf{B}(\mathbf{r})$ by

$$\iota = \arccos(B_c/B) \tag{9.27}$$

where B_c is the projection of $\mathbf{B}$ onto the Jovigraphic equatorial plane. The longitudes toward which the asymptotic lines point are $\lambda' = \phi \pm \xi$, where $\xi = \arcsin(B_\phi/B_c)$ and B_ϕ is the ϕ component of $\mathbf{B}$ at the apex of the cone (in a right-handed spherical coordinate system). The plus and minus signs refer to the southern hemisphere and northern hemisphere, respectively. The apparent source locations at the apex of the cone are then $\Lambda(\pm) = \lambda' \pm \mu$, where here the plus and minus refer to the two sides of the conical sheet.

If we now consider radiation coming from conical sheets aligned along only one magnetic flux tube, then at a particular time an observer may be receiving radiation from two or one (degenerate case) emission cones originating from different positions along the field line. Because the radiation is emitted close to the electron cyclotron frequency, two (or one) frequencies will be seen at that time on a frequency-time spectrogram. As Jupiter rotates, the observation geometry changes and a succession of active flux tubes will come into view. When the resulting pattern is computed using the formulas given above, the frequency-time spectrogram shows an arc structure. The shape of this arc will depend on where in the magnetosphere the active flux tube is located and on the magnitude of the emission cone angle ψ.

Pearce [1981] and Goldstein and Thieman [1981] have both tried to compare their calculations directly with dynamic spectra obtained from the Voyager PRA experiment. Pearce used a dipole approximation to the Jovian magnetic field and assumed that ψ remained constant at all frequencies along a given arc. He then attempted to find a source location and cone angle which would provide a good fit to selected observations. A typical result of such a calculation is shown in Figure 9.8, taken from Pearce [1981]. In the figure the cone is located on the $L = 5.5$ flux tube and ψ is 18°. The calculation assumes that the observer is at 30° south latitude. During the time the observations were taken, the Voyager spacecraft was actually at 5° north latitude. Thus, Pearce's analysis seems to be internally inconsistent. In addition, the constant and small value of ψ implies that sources A and B are independent and could not represent opposite sides of the same conical emission pattern.

Goldstein and Thieman take a somewhat different approach. In contrast to Pearce, for whom the L shell of the source is a variable, Goldstein and Thieman assume that the active field lines are at $L = 6$, i.e., that the radiation is stimulated by the motion of Io. They also assume that the O4 octupole model provides a reasonably accurate representation of the magnetic field. In this case the computed "arcs" resemble the observed

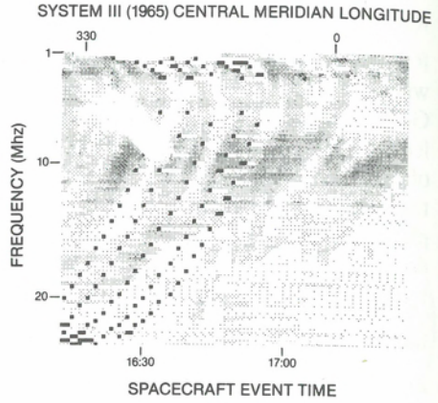

Fig. 9.8. Arc model predictions (black squares) superimposed on Voyager 1 data from February 10, 1979. The model calculation placed the source on the $L = 5.5$ flux tube and assumed a half angle for the conical emission pattern of $\psi = 18°$. A dipole approximation was used for the Jovian magnetic field. [Taken from Pearce, 1981.]

dynamic spectra only if the cone angle varies with frequency. They argue that refraction of the electromagnetic wave when it is close to ω_R could change ψ in the proper way. An example of the type of fit to the data that can be obtained if ψ varies with frequency while the observer is constrained to the equatorial plane is shown in Figure 9.9, taken from Goldstein and Thieman [1981]. This model requires somewhat different sets of input parameters to fit the main and early sources (A and B, respectively), and to differentiate between "greater" and "lesser" arcs. The model could be improved by incorporating growth rates and refraction predicted by a specific instability mechanism. However, fitting the longitude of the highest frequencies in source B may still be difficult. It is not clear whether the basic interpretive model is at fault, or whether the discrepancies would be removed if only a more detailed model of the magnetic field near the ionosphere were available.

Staelin [1981] and Hewitt, Melrose, and Rönmark [1981] have ascribed the variation of ψ with frequency to the way in which the relativistic resonance condition (9.4) and the variation of the maximum unstable wave number with frequency will change with both cyclotron frequency and the ratio ω_{pe}/ω_{ce}.

None of these arc models directly addresses the question of why the arcs appear discrete on the dynamic spectra. Boischot and Aubier [1981] have argued that the discreteness can arise from destructive interference between neighboring flux tubes, even if all field lines are emitting simultaneously. For this to work, the emission mechanism would have to produce coherent waves, which has not been a feature of the theories developed thus far. Nonetheless, by suitable variation of the relative phases of the interfering waves with frequency and time, Boischot and Aubier claim to be able to explain not only the discreteness of the arc pattern, but also the shapes of the arcs.

Gurnett and Goertz [1980a] attribute the discreteness to the nature of the interaction of the current carrying Alfvén wave with the ionosphere and torus. They point out that after the Alfvén wave is reflected from the ionosphere it is not expected to arrive back at the orbit of Io in time to close the dc circuit [Neubauer, 1980]. Therefore, many reflections of the wave could occur between hemispheres, thereby producing an extended standing wave current system downstream of Io. The three-dimensional geometry of this current system is illustrated in Figure 9.10. The apparent change in slope of the wave trajectory at the boundary of the torus is caused by the much lower plasma density outside of the torus. Because the reflected waves essentially produce a series of mirror images of the original Alfvén wave current system extending all around the Io L shell, this system of multiple reflections provides a simple explanation for the large number of decametric arcs observed in the radio emission spectrum

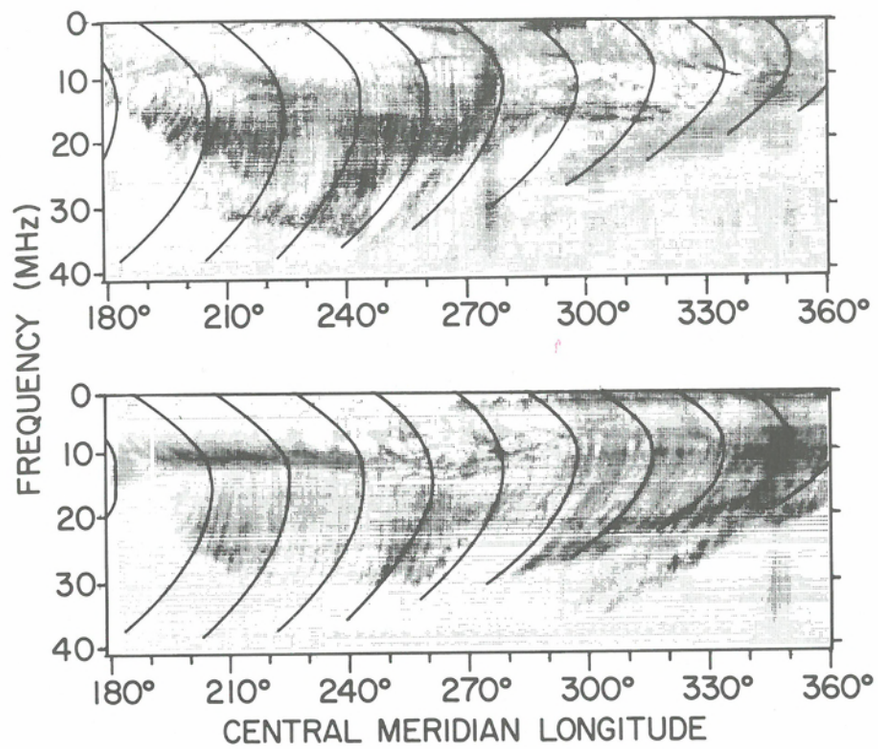

Fig. 9.9. An overlay of the modeled arcs on dynamic spectra observed by Voyager 2 on July 6–7, 1979 (upper panel), and July 3, 1979 (lower panel). The upper panel is an example of an Io- dependent source A event (the phase of Io is 240° when the central meridian longitude is 212°). The lower panel is an example of an Io-dependent source C event centered around 330° (Io phase is 240° at a longitude of 329°). The model calculation placed the source on the $L = 6$ flux tube and the half angle of the conical emission pattern varied as a function of frequency as described in the text. The O4 magnetic field model was used in these calculations [from Goldstein and Theiman, 1981].

(Chap. 7). In the figure, $\Delta\phi_0 = (360°)\cdot(2\ell M_A) / 2\pi(5.9R_J)$. Using 0.15 for M_A, the Alfvén mach number in the torus, and $2R_J$ for ℓ, the thickness of the torus, the longitudinal separation between successive reflections is $\Delta\phi_0 \simeq 5.8°$. There is also a minor periodicity $T_1 = (\Delta\phi_1/\Delta\phi_0)T_0$ introduced by the out-of-phase wave propagating in the opposite direction away from Io. Gurnett and Goertz [1980a] estimate that a large number (more than 10) of wave reflections could occur before the wave is damped by collisions in the ionosphere or collisionless processes in the magnetosphere, and that the temporal separation between successive arcs will range from 0 to 40 min.

Recently, Warwick [1981] has approached the problem of why the arcs are discrete by abandoning the hypothesis that the emission is directly related to the Jovian magnetic field as modeled by Pioneer 11 measurements. He attributes the sequence of arcs to a manifestation of widespread fine structure in the magnetic field. This fine structure is assumed to have dimensions similar in size and shape to the white ovals on the visible disk of Jupiter. Because this model is not related to the multipole models of the main Jovian magnetic field, it has the potential for accounting for the Io controlled source B location, which, as we have mentioned, has proved very difficult to explain in

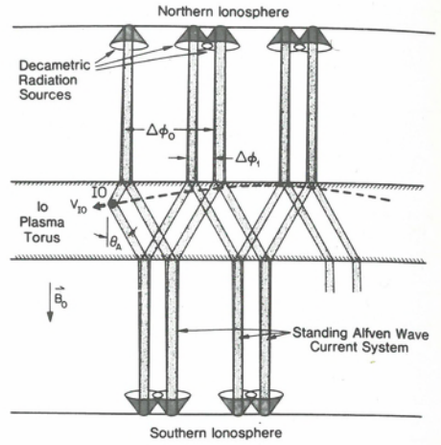

Fig. 9.10. A schematic sketch of the current system that might arise from the interaction of Io with the Jovian ionosphere and plasma torus. The current is carried by an Alfvén wave that is reflected from the ionosphere. If the reflected wave does not close the dc circuit by returning to Io, the possibility arises that many reflections of the wave could occur between the northern and southern ionospheres and the torus, thereby providing a possible explanation for the discrete arc pattern that characterizes the decameter radiation [from Gurnett and Goertz, 1981].

models which do attribute the source locations to properties of the global magnetic field. Several aspects of this model will have to be investigated in greater detail before its relationship to the observations is understood. For example, it is by no means obvious that the upper Jovian atmosphere can support islands of magnetic field signficantly more intense than in the surrounding medium; nor has it been conclusively demonstrated that the hypothesized field strengths could not in fact have been observed by Pioneer 11. Perhaps the most puzzling aspect of Warwick's model is that it divorces the observed decameter morphology from nearly all observable aspects of the magnetic field, in spite of the rather promising progress that has been made in our understanding of many phenomena (not withstanding the location of the Io-B source) utilizing the multipole models of the global magnetic field.

Implicit in the foregoing discussion of decameter arcs has been the assumption that a single large source region or a series of many small sources are radiating simultaneously to produce the large longitudinal extent of the decameter radiation. The individual sources are known from Very Long Baseline Interferometry (VLBI) to be quite small with projected linear dimensions along the line of sight less than 400 km [Dulk, 1970; Lynch et al., 1972]. This suggests that there must be multiple sources to account for the large longitudinal extent of the emission. That this is not necessarily the case has become evident from a rather novel interpretation of the arc pattern suggested by Lecacheux, Meyer-Vernet, and Daigne [1981]. In their model, the entire longitudinal extent of the emission can arise from a single small source located along a single field line.

The essential new feature in this theory is the inclusion of diffraction effects on the radiation as it propagates through the plasma torus near Io's orbit (see Chaps. 3, 6, and 11 for a description of properties of the torus). Lecacheux et al. argue that the plasma torus acts as a thin screen, changing the phase of the radio waves as in Fresnel diffraction. The resulting diffraction fringes, shown in Figure 9.11, resemble a pattern of arcs, either vertex early or vertex late, not dissimilar from the observed patterns. A careful comparison between the observations and this theory remains to be carried out, but it does seem clear that a pattern of repeating arcs can in principle be produced by a single localized source. Beaming of the radiation into a hollow conical sheet still appears to be required if sources A and B are to be interpreted as coming from the same physical location.

If the diffraction hypothesis is correct, then during the closest approach of Voyager 1, when the spacecraft was actually inside the Fresnel screen, the arc pattern

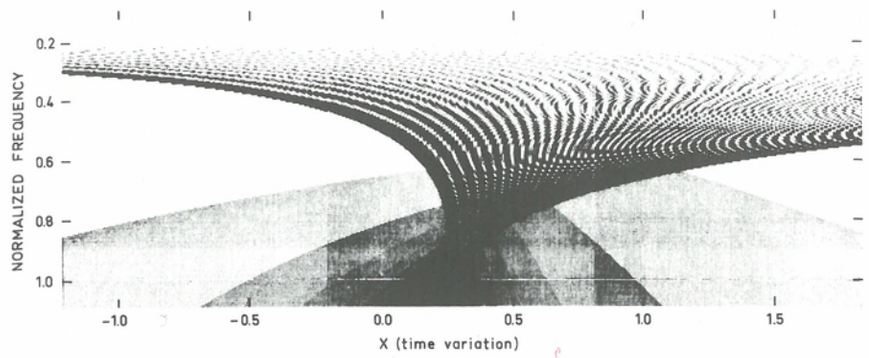

Fig. 9.11. Computed fringe patterns are shown for a ray tracing calculation in which the Io plasma torus is treated as a thin Fresnel screen. The frequency-time plot illustrates the intensity enhancements resulting from Fresnel diffraction of decameter waves [from Lecacheux et al., 1981].

should have disappeared. The observations do not suggest a clearcut resolution of this question, for although much of the familiar early and main source radiation is absent, some arcs are still present in the dynamic spectra [J. Alexander, private communication]. As far as we know, the close encounter data have not yet been analyzed in the context of any of the arc models.

9.5. Summary

In the previous sections we have concentrated on one question: What requirements can theory put on the particle distribution function necessary for the generation of DAM (or HOM and KOM for that matter)? The conclusion from our discussion must be that any anisotropic distribution of energetic particles can, in principle, be unstable against the emission of the fast X-mode, the most likely candidate for DAM. Direct mechanisms usually require a loss-cone type distribution whereas indirect mechanisms require a beamlike distribution for the generation of electrostatic waves that in turn produce the electromagnetic waves by one or another three-wave coupling mechanisms. This state of affairs is, of course, quite unsatisfactory, but it is very unlikely that we will ever know much more about the in situ plasma conditions including the existence or non-existence of particular electrostatic wave modes in the generation region of DAM. However, the similarity between DAM and TKR suggests that an understanding of TKR will also help to explain DAM. Obviously, such a view cannot be defended rigorously.

As yet there is no completely convincing theory of TKR (the problem being uniqueness not correctness) and so we cannot simply conclude that DAM is generated by exactly the same process, whatever that may be. Furthermore, there are significant differences between DAM and TKR, including the role of Io, spectral arcs, as well as the probability that although the source region of DAM is underdense in the sense $\omega_{pe}/\omega_{ce} << 1$, the ambient density still exceeds the beam density. Based on the discussions in Sections 9.3 and 9.4, we feel that the prominent Io-phase control of DAM is easier to understand if an indirect generation mechanism is operating. The argument is twofold. The highest DAM frequency of 39.5 MHz suggests generation in the northern hemisphere on field lines that connect Io to a region where the magnetic field is 14 G. Such a large field exists only in the northern hemisphere according to the presently known field models. If Io were only to enhance the pitch angle scattering of a

trapped particle distribution into the loss-cone, the particles would precipitate into the southern hemisphere where the field is low [see Roederer, Acuña, and Ness, 1977; Dessler and Hill, 1979; Goldstein and Eviatar, 1979]. If, on the other hand, Io stimulates the generation of an electron beam, particles could reach the high magnetic fields in the northern hemisphere. One mechanism by which Io can generate beamlike distributions has been discussed in Section 9.4.

Clearly neither of these arguments are completely compelling. Even a precipitating beamlike distribution is capable of exciting loss-cone instabilities because the albedo distribution can resemble a loss-cone. Thus, even observation of electron beams would not necessarily provide a definitive resolution to this question. Furthermore, in neither of the four Jupiter fly-bys has there been clear indication of an Io injected electron beam, although the trajectories, viewing geometry and instrumentation have not been completely optimal. The same can be said about the existence or nonexistence of loss-cone features in the electron distribution.

We have briefly discussed some of the morphological aspects of DAM. Again we are faced with the problem of uniqueness. A case in point is the explanation of the decametric arcs in terms of at least three completely different models. However, more refined Earth based VLBI observations of DAM may distinguish between the models that require either one large or several small sources. It cannot be stressed enough that our ignorance about the source position and size is still the most serious obstacle to understanding DAM.

From our discussions and those in Chapter 7, it has become clear that the Io control consists essentially in the enhancement of a nearly continuous source. Either Io's influence extends over large distances away from Io as in the model of Gurnett and Goertz [1981], or as Io approaches this continuously active source, it only enhances the source intensity. Such an enhancement might be variable and related to the amount of plasma or neutrals Io injects into the torus region. Because the neutral and plasma density influences the intensity and spectral characteristics of the optical emission from the Io torus, there may be a correlation between the observed variability of the optical emission and DAM. If such a correlation exists, it would be an important clue to the understanding of DAM and the Io effect.

It is to be expected that neither the morphology nor the phenomenology of DAM will definitively distinguish between existing models. What is needed at this stage is, simply, a more detailed formulation of all the various theoretical models, more specific calculations to determine the range of parameters that each model can tolerate, more detailed estimates of the efficiency of each mechanism utilizing detailed global magnetic field and density models and the continuing effort to formulate observational tests of the models. Finally, we remark that the recent kilometric radiation from Saturn (SKR) by Kaiser et al. [1980] suggests that the emission of radio waves is a general feature of planetary magnetospheres. Perhaps by comparative study, we will be able to eliminate some presently viable theories. Although that will be difficult, the reward of understanding such an enigmatic phenomenon as planetary radio emission will be high.

APPENDIX

We first derive the probability of spontaneous wave emission by a single particle. Then, by integrating over a distribution of particles, emission from all particles can be computed. By use of the Einstein relations, and a similar integration over the particle distribution, we then calculate the coherent, or stimulated, emission.

We assume that the dielectric tensor $\epsilon_{ij}(\mathbf{k},\omega)$ for the background medium is Hermitian (no damping) and given by cold plasma theory [Stix, 1962]. When the Maxwell equations are Fourier transformed the results can be written in the form of an equation for the wave electric field $\mathbf{E}$

$$\Lambda_{ij}(\mathbf{k},\omega)E_j(\mathbf{k},\omega) = -\frac{4\pi i}{\omega} j_i(\mathbf{k},\omega) \tag{A.1}$$

where summation over repeated indices is assumed and $\mathbf{j}$ is a source current.

The tensor Λ_{ij} is related to the refractive index $n \equiv kc/\omega$ by

$$\Lambda_{ij}(\mathbf{k},\omega) = n^2(K_i K_j - \delta_{ij}) + \epsilon_{ij}(\mathbf{k},\omega) \tag{A.2}$$

$$\mathbf{K} = \mathbf{k}/k, k = |\mathbf{k}|$$

The current $\mathbf{j}$ could arise from either an uncorrelated random motion of charged particles, producing incoherent radiation; or an ordered motion producing coherent radiation. The average power radiated by $\mathbf{j}$ is given by

$$P = -\lim_{T\to\infty} \frac{1}{T} \int_{-T/2}^{T/2} dt \int d^3r\ \mathbf{j}(\mathbf{r},t) \cdot \mathbf{E}(\mathbf{r},t) \tag{A.3}$$

The radiation can thus be thought of as a dissipation of particle energy. The physical interpretation of Equations (A.1) and (A.3) is then transparent. A free current generates electric fields in a medium described by the dielectric tensor ϵ_{ij}. The power radiated is then equal to the energy loss $\mathbf{j}\cdot\mathbf{E}$. Expressing $\mathbf{j}$ and $\mathbf{E}$ in terms of their Fourier transforms and using the fact that negative and positive frequencies are physically equivalent we obtain

$$P = -\int d^3k \int_0^\infty d\omega[\,\mathbf{j}^*\cdot\mathbf{E} + \mathbf{j}\cdot\mathbf{E}^*]/(2\pi)^4 \tag{A.4}$$

The formal solution of (A.1) is

$$E_i(\mathbf{k},\omega) = -\frac{i}{\omega} D_{ij}(\mathbf{k},\omega)\, j_j(\mathbf{k},\omega) \tag{A.5}$$

where the dispersion tensor is

$$D_{ij} = 4\pi\lambda_{ij}(\mathbf{k},\omega) / \Lambda(\mathbf{k},\omega) \tag{A.6}$$

and $\lambda_{ij}(\mathbf{k},\omega)$ is the cofactor of Λ_{ij} defined by $\Lambda_{ij}\,\lambda_{jl} = \Lambda\delta_{il}$, $\Lambda(\mathbf{k},\omega)$ is the determinant of $\Lambda_{ij}(\mathbf{k},\omega)$. For normal modes $\Lambda = 0$ and D_{ij} is singular. The integration around this singularity is well known in plasma physics [see, e.g., Krall and Trivelpiece, 1973]. Because we are interested in $\mathbf{E}(t)$ due to the current $j(t_o)$ for $t_o < t$, we use retarded functions and integrate above the singularity $\omega = \omega(\mathbf{k})$ (or equivalently give ω a small positive imaginary part). Then

$$D_{ij} = \frac{4\pi\lambda_{ij}}{\partial\Lambda/\partial\omega}\left\{ P\frac{1}{\omega - \omega(\mathbf{k})} - i\pi\delta[\omega - \omega(\mathbf{k})] \right\} \tag{A.7}$$

The principal part does not contribute to the integral in Equation (A.4), and thus

$$P = \frac{1}{2\pi^2} \int d^3k \int (d\omega/\omega)\ \frac{|\lambda_{ss}|\ |\hat{e}_i\, j_i^*|^2\, \delta[\omega - \omega(\mathbf{k})]}{\partial\Lambda/\partial\omega} \tag{A.8}$$

where $\hat{e} = \mathbf{E}/|\mathbf{E}|$ is the polarization vector of the wave, and λ_{ss} is the trace of λ_{ij}. This result holds for any current. We now let the current arise from a particle of charge q and mass m, that is,

$$\mathbf{j}(\mathbf{r},t) = q\mathbf{v}(t)\delta[\mathbf{r} - \mathbf{r}(t)] \tag{A.9}$$

where the particle's trajectory $\mathbf{r}(t)$ and the velocity $\mathbf{v}(t)$ satisfy the equation of motion in a uniform, unperturbed, magnetic field.

We choose a coordinate system in which $\mathbf{k} = (k_\perp, 0, k_\parallel)$. Then the Fourier transform of $\mathbf{j}$ is [Melrose, 1968]

$$j_i(\mathbf{k},\omega) = \frac{\pi|q|c^2}{(m^2c^4 + p^2c^2)^{1/2}} \sum_{\nu=-\infty}^{\infty} \left(\frac{q}{|q|} \frac{k_\perp}{|k_\perp|} \right)^{\nu+1} \Gamma_i^\nu \, \delta(\omega - \nu\Omega - k_\parallel v_\parallel) \tag{A.10}$$

The quantities Γ_i^ν are related to the Bessel functions $J_\nu(z)$ and their derivatives $J'_\nu(z)$ via the following relationships

$$\Gamma_1^\nu = 2p_\perp(\nu/z)\, J_\nu(z) \tag{A.11}$$

$$\Gamma_2^\nu = -2ip_\perp(q/|q|)\, J'_\nu(z)$$

$$\Gamma_3^\nu = 2p_\parallel(k_\perp/|k_\perp|)\, J_\nu(z)$$

where $z = k_\perp v_\perp / \Omega = k_x p_x / m\omega_c$, $\omega_c = |q|B/mc$ is the cyclotron frequency of the species of interest, $\Omega = \omega_c/\gamma_r$, and $\gamma_r = (1 - v^2/c^2)^{1/2}$. One should note that unlike the situation in the Earth's magnetosphere, the relativistic treatment is sometimes necessary in the Jovian magnetosphere where particles can often be accelerated to high energies [see, e.g., Wu and Freund, 1977; Sentman and Goertz, 1978]. After inserting Equation (A.10) into (A.8) the power reduces to

$$P = \sum_{\nu=-\infty}^{\infty} \frac{q^2c^2}{4\pi(m^2c^4 + p^2c^2)} \tag{A.12}$$
$$\cdot \int d^3k \int (d\omega/\omega)\, |\lambda_{ss}|\, |\hat{e}_i\Gamma_i^{\nu *}|^2 \delta(\Lambda)\delta(\omega - \nu\Omega - k_\parallel v_\parallel)$$

In (A.12) the first delta function expresses the fact that we are calculating the power radiated into a particular cold plasma mode ($\Lambda = 0$), and the second delta function expresses a resonance condition for the parallel velocity.

The time average power radiated into a mode $\omega(\mathbf{k})$ can also be defined in terms of the following quantum-mechanical analog. Assume that a particle is in a quantum state s corresponding to a momentum $p_\parallel$ and $p_\perp$ where

$$p_\perp{}^2 = (qB/c)\hbar(2n + 1) \tag{A.13}$$

$$s = \{p_\parallel, n\}$$

Note that for all practical purposes the quantization step $\Delta p_\perp{}^2 = (qB/c)\hbar$ is negligibly small and the quantum states really form a continuum.

We define the probability of spontaneous emission $w_s^{s'}(\mathbf{k})$ as the probability that a particle in state s emits a photon $\hbar\omega$ with transition to s'. Then

$$P = \sum_{s'} \int \frac{d^3k}{(2\pi)^3} \hbar\omega(\mathbf{k}) w_s^{s'}(\mathbf{k}) \tag{A.14}$$

where the sum is over all possible final states. If we use

$$s' = \{p_\parallel - \hbar k_\parallel, n - \nu\}$$

then we can rewrite (A.14) as

$$P = \sum_{\nu=-\infty}^{\infty} \int \frac{d^3k}{(2\pi)^3} \hbar\omega(\mathbf{k}) w(\mathbf{k})_{p_\parallel, n, \nu} \tag{A.15}$$

From (A.12), we obtain for the transition probability

$$w(\mathbf{k})_{p_\parallel, n, \nu} = \frac{2\pi^2q^2c^4}{\hbar(m^2c^4 + p^2c^2)} \int \frac{d\omega}{\omega^2} |\lambda_{ss}|\, |\hat{e}_i\Gamma_i^{\nu *}|^2 \delta(\Lambda)\delta(\omega - \nu\Omega - k_\parallel v_\parallel) \tag{A.16}$$

In this quantum-mechanical description the distribution function $f(\mathbf{p})$ of the particles is replaced by $f(s)$, the occupation number of each momentum state s, so that

$$\frac{1}{V} \Sigma f(s) = \text{particle number density} \tag{A.17}$$

where V is the total volume of the system. Similarly, the photons have a distribution $N(\mathbf{k})$ and momentum $\hbar\mathbf{k}$ given by

$$\int \frac{d^3k}{(2\pi)^3} N(\mathbf{k}) = \text{photon number density} \tag{A.18}$$

The rate of increase in the density of the waves due to spontaneous emission is then

$$\frac{\partial N^{se}}{\partial t}(\mathbf{k}) = \frac{1}{V} \sum_{s,s'} s_s^{s'}(\mathbf{k}) f(s) \tag{A.19}$$

The classical limit can be recaptured by using the replacements

$$\frac{\Sigma f(s)}{V} \to \int d^3p f(\mathbf{p})$$

and

$$w_s^{s'}(\mathbf{k}) \to w(\mathbf{k})_{p_\parallel, n, \nu} \tag{A.20}$$

so that the spontaneously generated wavepower $[N\hbar\omega(\mathbf{k})]$ is

$$\frac{\partial P^{se}}{\partial t} \equiv \alpha(\mathbf{k}) = \sum_\nu \int d^3p f(\mathbf{p}) \frac{2\pi^2q^2c^4}{(m^2c^4 + p^2c^2)} \tag{A.21}$$
$$\int \frac{d\omega}{\omega} |\lambda_{ss}|\, |\hat{e}_i\Gamma_i^{\nu *}|^2 \delta(\Lambda)\delta(\omega - \nu\Omega - k_\parallel v_\parallel)$$

For induced processes (coherent interactions), the change in $N(\mathbf{k})$ is given by the difference between the rate that photons with momentum $\hbar\mathbf{k}$ are emitted and the rate they are absorbed. The Einstein relations state that the probability of induced emission and absorption, $s \to s'$ and $s' \to s$, respectively, are both equal to $w_s^{s'}(\mathbf{k})\, N^{ie}(\mathbf{k})$. Thus, for induced processes,

$$\frac{\partial N^{ie}}{\partial t}(\mathbf{k}) = \frac{1}{V}\sum_{s,s'} w_s^{s'}(\mathbf{k}) N^{ie}(\mathbf{k})[\, f(s) - f(s')\,] \tag{A.22}$$

Again taking the classical limit, we obtain for the sum of coherent and incoherent emission, (see Melrose [1968] for details)

$$\frac{\partial P}{\partial t}(\mathbf{k}) = \sum_{\nu} \int d^3p\,[\,(1 + (1/2)\,D_\nu)\, w(\mathbf{k})_{p_\parallel, n, \nu}\, P(\mathbf{k})\,]\, D_\nu f(\mathbf{p}) \tag{A.23}$$

$$+ \frac{\partial P^{se}}{\partial t} = \gamma(\mathbf{k}) P(\mathbf{k}) + \alpha(\mathbf{k})$$

where

$$D_\nu = \hbar \left[\frac{\nu \omega_c m}{p_\perp} \frac{\partial}{\partial p_\perp} + k_\parallel \frac{\partial}{p_\parallel} \right]$$

A Taylor expansion of $f(s')$ has been used in deriving (A.23). The expression for the growth rate $\gamma(\mathbf{k})$ can now be found from (A.23) for D_ν under the assumption that $f(\mathbf{p})$ is gyrotropic, the quantum correction $(1/2)D_\nu$ is negligible, and $w(\mathbf{k})$ is given by (A.16). The final result is Equation (2.1).

Under many conditions one can also show [Kennel, 1966; Melrose, 1968; Hasegawa, 1975]

$$\gamma(\mathbf{k}) = Im\,[\Lambda(\mathbf{k},\omega)] \,/\, \{\partial Re\,[\Lambda(\mathbf{k},\omega)/\partial\omega]\} \tag{A.24}$$

10
MAGNETOSPHERIC MODELS

T. W. Hill, A. J. Dessler, and C. K. Goertz

Theoretical ideas concerning Jovian magnetospheric phenomena are at least as diverse as the phenomena themselves, and there presently exists no single comprehensive model that encompasses all known phenomena within a unified theoretical framework. We identify here a number of important theoretical concepts, some subset of which (together with perhaps others yet unidentified) will ultimately provide the elements of such a comprehensive model. A number of ideas have been advanced to account for the copious plasma source associated with Io, but none of these has yet accounted satisfactorily for both the magnitude and the morphology of the inferred source. Nevertheless, given the observed fact that Io supplies the bulk of the magnetospheric plasma mass, and the corollary that the net plasma transport is predominantly outward, it follows that the rotational energy of Jupiter is an important if not dominant source of energy for magnetospheric phenomena. This rotational energy is expended in a variety of phenomena, including the electrodynamic Io–Jupiter interaction and associated radio and auroral emissions, the acceleration of charged particles to MeV energies, and the generation of a wide variety of spin-periodic phenomena as observed both remotely and in situ. The spin periodicities observed within the magnetosphere can be explained for the most part as resulting from the diurnal wobble of the magnetospheric current sheet caused by the offset between Jupiter's magnetic dipole axis and its spin axis. However, remotely observed spin periodicities (the "pulsar" phenomena) apparently require the existence of an intrinsic longitudinal asymmetry in the Jovian magnetosphere that corotates with Jupiter.

10.1. Introduction

Many celestial bodies have magnetospheres, that is, surrounding regions within which the motion of charged particles is influenced by the magnetic field of the central body. In addition to the terrestrial magnetosphere, which has been studied in increasing detail over the past three decades, the magnetospheres of Mercury, Jupiter, and Saturn have now been explored in situ. The Sun has a magnetosphere of sorts (the heliosphere), and there is evidence that pulsars, accreting binary star systems, and certain radio galaxies also have magnetospheres. Of the planetary magnetospheres that have been explored, Jupiter's is by far the largest in terms of both absolute size and size relative to the planetary body. It is also a magnetosphere largely dominated by rotational effects; as such, it offers unique insight to the study of inaccessible pulsar magnetospheres.

The present state of knowledge of Jupiter's magnetosphere is reminiscent of the state of knowledge of Earth's magnetosphere in the early 1960s – the observational data are sufficient to inspire a variety of theoretical developments but not sufficient in most cases to dictate a clear choice among them. Future observations will probably verify some of the theoretical concepts described below, and will probably disprove others. We shall concentrate here on those theoretical concepts that we believe to be consistent with available observations as described elsewhere in this book, and we shall explicitly point out areas of divergent views or inadequate study.

Our data base is relatively incomplete in coverage (local time, latitude, time, etc.), compared to the terrestrial magnetospheric data base, but there is a tendency to suppose that we can learn more now from a limited data base by drawing on several years'